WILEY | Hindawi

Research Article

Bridge Damage Detection Using Ambient Loads by Bayesian Hypothesis Testing for a Parametric Subspace of an Autoregressive Model

Yoshinao Goi [iD] **and Chul-Woo Kim**

Department of Civil and Earth Resources Engineering, Kyoto University, Kyoto 6158540, Japan

Correspondence should be addressed to Yoshinao Goi; goi.yoshinao.2r@kyoto-u.ac.jp

This study explores a change detection method in modal properties to automate and generalize in-service damage detection for vibration-based structural health monitoring of bridges. The noisy conditions caused by ambient loading pose difficulty for in-service damage detection because the load-induced noise often masks the difference in the modal properties. The proposed method directly converts measured time series into a simplified anomaly indicator robust against load-induced noise. This study adopts a vector autoregressive model to represent the vibration of bridges. Bayesian inference produces a posterior probability distribution function of the model parameters. Principal component analysis extracts a subspace comparable to the modal properties in the model parameters. Bayesian hypothesis testing quantifies anomalies in the extracted subspace. The feasibility of the proposed method is assessed with vibration data from field experiments conducted on an actual steel truss bridge. The field experiment includes damage severing the truss members. The modal frequencies and mode shapes estimated from the principal component analysis correspond well to earlier reported results. The proposed damage detection method successfully indicated all damage considered in the experiment.

1. Introduction

1.1. Background. Aging infrastructure management is a crucially important issue confronted by civil engineering professionals. Today, they adopt periodic visual inspection-based bridge management as a fundamental method of investigating the structural integrity of bridges. Structural health monitoring (SHM) provides a research field for nondestructive evaluation based on physical measurements and computer analyses to complement the existing inspection methods. Especially, vibration-based SHM has the advantage that a few sensors enable assessment of the condition of the whole structure because a local stiffness change affects the global dynamic characteristics represented by modal properties [1–3]. Two commonly used means to identify modal properties are input-output estimation and output-only estimation [3]. For input-output estimation, bridges are excited under controlled input signals. Contrary, bridges are excited by uncontrolled ambient loads such as traffic, wind, and ground motion for output-only estimation. We also refer to the output-only methods as operational modal analysis (OMA) methods because they enable the identification of modal properties solely from the measurable outputs under operation without traffic interruption. The ambient loads are usually modeled as steady white noise in most OMA methods since the external force is unknown in advance. We expect to apply OMA for damage detection as a screening method for numerous bridges without traffic interruption. However, as discussed below, noisy conditions caused by ambient loads still require effort for calibration and computation to automate damage detection.

Aiming damage detection using OMA, most earlier studies have adopted statistic change detection in modal properties, such as modal frequency, mode shapes, and

damping ratios [4–14]. Among them, Gudmundson [6] theoretically demonstrated that cracks and notches in a beam alter modal frequencies. Pandey et al. [7, 8] proposed to detect local changes in flexural stiffness using the curvature of mode shapes. Deramaeker et al. [9] demonstrated the feasibility of output-only modal estimation for vibration-based SHM under environmental changes with sensitivity analysis using a numerical model. For actual bridges in the field, the authors [10, 11] reported that they detected changes in modal properties caused by damage from vehicle-induced vibration. Several studies investigated the feasibility of OMA for the long-term monitoring of bridges under operation. Peeters and De Roeck [12] applied black-box models for one-year bridge monitoring data and distinguished damage-induced frequency changes from environmental-induced changes. Ni et al. [13] reported a change in dynamic behavior between ambient vibration and typhoon-induced vibration. Although environmental fluctuation changes modal properties, damage-induced fluctuation would be distinguished from environmental effects if we have enough prior knowledge and apply an appropriate change detection procedure. However, engineers must also consider that the load-induced noise often masks modal estimation because it engenders unrealistic modal properties estimators [10, 11, 14]. That is because ambient loads are modeled as steady white noise in most OMA methods, whereas ambient loads are often unsteady and colored noise. Therefore, they need to remove the unrealistic estimators caused by the masking effect of ambient loads.

The following feature extraction techniques are required to avoid the masking effect and distinguish the physically meaningful modes from the meaningless estimators: the frequency domain OMA requires preliminary calibration for peak-pick [15]. In time domain OMA, they usually need thresholds of modal validation criteria for stabilization diagrams [3]. In recent studies, Mao et al. [16] proposed to automate modal identification with hierarchical clustering and principal component analysis (PCA) in addition to the classical stabilization diagrams. In the previous study, they applied PCA to reduce the dimension of modal validation criteria beforehand the clustering process. Engineers can compare modal properties estimated with the above-mentioned feature extraction techniques for damage detection. However, they still need to apply statistical methodology such as hypothesis testing because each modal property involves variance caused by the estimation error. Also, they are often required to choose modal properties for comparison because the modal properties irrelevant to the damage decrease the sensitivity of the hypothesis test. The comparison requires engineers' experience both for hypothesis testing and for modal analysis, and thus the results of damage detection depend on the skill of the engineers. A subjective judgment made by inexperienced engineers may cause a false alert or overlook failure. Accordingly, it is still challenging to generalize and automate the procedure required for change detection in modal properties.

Nair et al. [17] proposed omitting modal estimation procedures for damage detection to automate damage detection. They applied anomaly indicators converted from a univariate AR model instead of modal properties. The feasibility of the anomaly indicator has been examined for a modeled bridge [18] and an actual steel truss bridge [19]. Zhang [20] also proposed a statistical diagnosis procedure by change detection in the AR model. The proposed procedure examines the difference in residuals in the AR models. For multipoint measurement, the authors [21] expanded these previous studies and proposed an anomaly indicator calculated from a vector autoregressive (VAR) model instead of a univariate AR model. In the study, the authors carefully chose the AR order to avoid the masking effect caused by the load-induced noise. That is because the load-induced noise produces physically meaningless estimators in the AR coefficients. The practical application of AR-model-based anomaly indicators is consequently limited so far. For an anomaly indicator robust against ambient loads, we desire to extract physically meaningful parameters from the VAR model and cancel out the masking effect caused by the meaningless VAR coefficients. This study applies Bayesian statistics to quantify the uncertainty involved in VAR coefficients and proposes a methodology to cancel them out. In a Bayesian manner, the procedure to adjust the AR order is also automated and generalized. Furthermore, this paper applies PCA to extract the physically meaningful parameters relevant to classical modal analysis theory.

Bayesian statistics is a widely used methodology to quantify the uncertainty in stochastic model parameters. Several previous studies applied Bayesian inference [22] to quantify the uncertainty of modal properties. For instance, Yuen and Katafygiotis [23] and Au et al. [24] proposed a Bayesian modal analysis method. In the previous study, the posterior distribution of the parameters represents their uncertainty according to observed data. Lam et al. [25] applied this method to model updating, and the updated model was subsequently adopted for model-based damage detection. Some other previous studies applied Bayesian methodologies in various approaches for damage detection. For instance, Jiang and Mahadevan [26] proposed a Bayesian hypothesis testing [27] adopting a dynamic fuzzy wavelet neural network method for nonparametric damage detection. Sun et al. [28] proposed damage detection using a Bayesian information model, including local information such as static strain and deflection. Figueiredo et al. [29] applied Mahalanobis distance obtained from Markov chain Monte Carlo (MCMC) techniques as an anomaly indicator. Dzunic et al. [30] applied a Bayesian state-space approach and investigated multiclass classification for damage detection. The Bayesian stochastics is also available for machine learning providing decision-making strategies for damage detection. For instance, Silva et al. [31] adopted neural networks with autoencoders to extract damage-sensitive features. Arangio and Beck [32] utilized Bayesian neural networks and discussed their feasibility for SHM. In the recent advances in uncertainty quantification and machine learning, stochastic models tend to be detailed and complicated. Accordingly, some of the parameters that consist of the models and threshold are often required to be predefined. Also, most cases for recent Bayesian applications adopt iterative optimization methods such as MCMC

techniques. The computational resources needed in optimization are considerable for prompt decision-making in SHM. As discussed later, Bayesian inference for the VAR model applied in this paper enables much simpler computation because it has posterior distribution in closed form solution.

Recently, the novelty detection approach in machine learning has been applied to structural damage detection [33, 34]. In this sense, one-class classification formulates structural damage detection without prior knowledge of damages. This study concerns parametric change detection utilizing this approach. Damage detection methods proposed by Figueiredo et al. [29] and Dzunic et al. [30] mentioned above also apply this approach. Dimension reduction by PCA is one of the popular methodologies to extract physically meaningful parameters for change detection [35–37]. For instance, Akintude et al. [35] demonstrated that proper orthogonal modes from PCA of strain time history indicated damage in a full-scale bridge deck mock-up using variable vehicle loads and speeds. In the previous study by Mao et al. [16] mentioned above, PCA is applied to extract physically meaningful modes from stabilization diagrams. For anomaly detection of modal properties, Ozdagli and Kousoukos [36] investigated an indicator to detect changes in modal properties using reduced dimensions by PCA. PCA was also applied to distinguish damage-induced frequency change from environment-induced change. For instance, Sen et al. [37] applied PCA to modal frequencies to decouple structural damage and environmental effects. Furthermore, a classical modal analysis theory shows that the modal properties are also related to the PCA for a vector of the measured time series, as discussed in Appendix A. This study applies this result to extract damage-sensitive parameters for anomaly detection.

1.2. Outline of the Proposed Method. This study aims to provide an easy-to-use framework for change detection in modal properties with minimum adjustment. This study proposes a change detection method so that it meets all of the following conditions:

(i) An anomaly indicator is formulated based on hypothesis testing for convincing change detection

(ii) To automate and generalize the procedure for damage detection, the anomaly indicator is directly converted from the measured time series

(iii) Bayesian statistics is applied to quantify the uncertainty involved in the stochastic model

(iv) For fast computation, no iterative method is adopted for Bayesian inference

(v) Damage-sensitive parameters comparable to modal properties are extracted to avoid errors caused by parameters unrelated to modal properties

This study adopts a VAR model as a bridge vibration model under ambient loads. Even though a VAR model merely provides a rough approximation of the structural

responses, it still has an advantage in simple and fast computation. As discussed in Section 1.1, unsteady load-induced noise engenders meaningless estimators in the VAR coefficient. This study proposes the following framework to reduce the masking effect caused by ambient loads.

Bayesian inference for the VAR coefficients and the covariance matrix of the error term provide posterior distribution of the parameters. Because the posterior distribution is in closed form solution, the Bayesian inference is available without the iterative optimization. In the Bayesian inference, the prior distribution represents noninformative initial knowledge before measurement and the posterior distribution represents updated knowledge after measurement. Hyperparameters calculated from the measured time series represent the posterior distribution of the VAR coefficients and the covariance matrix. The posterior distribution quantifies the most probable values and uncertainty for each regressive parameter from the observation. An orthogonal basis derived from the PCA transforms the posterior distribution of VAR coefficients. The damage-sensitive parameters appear in a parametric subspace whose dimension the PCA reduces. Appendix A shows that the extracted damage-sensitive parameters are comparable to the modal properties estimated in a classical modal analysis method. Accordingly, the transformed posterior distribution separates the VAR coefficients into damage-sensitive and meaningless parameters. Bayesian hypothesis testing [27] is applied to detect changes in the damage-sensitive parameters. The hypothesis testing adopts two hypotheses representing the healthy and damaged state of the bridge. For both hypotheses, evidence functions represent the likelihood of the observed data. Here, one evidence function presumes changes in the damage-sensitive parameters, and the other assumes no change. Each evidence function marginalizes the uncertainty of the other meaningless parameters with integration. A Bayes factor, a ratio of the two evidence functions, indicates the changes. Accordingly, the proposed Bayes factor reduces the masking effect caused by ambient loads. In this study, the threshold for the log-scaled Bayes factor to detect damage is fixed at 0, as discussed in Section 3.

The above procedure comprises the following two steps:

Step 1: Reference Modeling

Acquire acceleration time series from a bridge under healthy conditions (designated as the reference dataset). According to the Bayesian inference, transform the reference dataset into hyperparameters. Find the optimal AR order by the Bayesian information criterion (BIC) [22, 38]. Extract the damage-sensitive parameters by PCA.

Step 2: Damage Detection

Acquire a new acceleration time series from the same bridge under unknown damage conditions (designated as the test dataset). Calculate hyperparameters of the evidence functions for the two hypotheses representing healthy and damaged states. The Bayes factor exceeds the threshold if it detects any changes in the damage-

sensitive parameters between the reference and test datasets.

Engineers can convert damage-sensitive parameters to modal properties through a relevant state-space model [39, 40] just after Step 1. This procedure helps them interpret the physical meaning of the damage-sensitive parameters. They can omit this procedure from the framework if they do not need the physical interpretation.

Figure 1 presents an outline of the proposed damage detection method. Here, the equation numbers appear in Section 2 and Section 3. Section 2 describes optimizing the stochastic model for Step 1 and modal estimation. In Section 3, we formulate hypothesis testing for Step 2. We validate the proposed method in Section 4 with a case study of a steel truss bridge in the field [41]. Furthermore, Appendix B provides a case study using an existing approach, i.e., Bayesian hypothesis testing without principal component analysis, for comparison.

2. Reference Modeling

2.1. VAR Model Expansion. This section presents a general description of the VAR model expanded to Bayesian statistics. Let a synchronized time series of the acceleration be measured at m measurement locations on a bridge. A zero-mean time series is produced by subtracting the mean value from the measured acceleration. Let $\mathbf{y}_k \in \mathbb{R}^{m \times 1}$ $(k = 1 \dots n)$ denote a column vector at the k-th time step of the zero-mean time series with components corresponding to the measurement locations. As mentioned in Section 1, most of the OMA methods assume the ambient loads as steady white noise. The VAR model with sufficient numbers of model order p approximates the time series obtained from a linear structural dynamic system excited by white noise [42]. The VAR model is given as

$$\mathbf{y}_k = \sum_{i=1}^{p} \boldsymbol{\alpha}_i \mathbf{y}_{k-i} + \mathbf{e}_k \ (\text{for } k = p+1, \dots, n). \quad (1)$$

In that equation, $\boldsymbol{\alpha}_i \in \mathbb{R}^{m \times m}$ represents the i-th AR coefficient matrix, and $\mathbf{e}_k \in \mathbb{R}^{m \times 1}$ denotes a zero-mean Gaussian white noise vector. Letting $\mathbf{Y} = [\mathbf{y}_1^T, \dots, \mathbf{y}_n^T]^T \in \mathbb{R}^{mn \times 1}$, $\mathbf{W} = [\boldsymbol{\alpha}_p, \dots, \boldsymbol{\alpha}_1] \in \mathbb{R}^{m \times mp}$ and $\boldsymbol{\phi}_k = [\mathbf{y}_{k-p}^T, \dots, \mathbf{y}_{k-1}^T]^T \in \mathbb{R}^{mp \times 1}$, equation (1) leads to the following probability density function (PDF).

$$p(\mathbf{Y} \mid \mathbf{W}, \boldsymbol{\Sigma}) = p(\boldsymbol{\phi}_{p+1}) \prod_{k=p+1}^{n} \mathcal{N}(\mathbf{y}_k \mid \mathbf{W}\boldsymbol{\phi}_k, \boldsymbol{\Sigma}). \quad (2)$$

Therein, $\boldsymbol{\Sigma}$ denotes the covariance matrix of $\mathbf{e}_k$; $p(\boldsymbol{\phi}_{p+1})$ denotes the PDF of $\boldsymbol{\phi}_{p+1}$; $p(\mathbf{Y} \mid \mathbf{W}, \boldsymbol{\Sigma})$ denotes the conditional PDF of $\mathbf{Y}$ conditioned by $\mathbf{W}$ and $\boldsymbol{\Sigma}$; $\mathcal{N}(\mathbf{y}_k \mid \mathbf{W}\boldsymbol{\phi}_k, \boldsymbol{\Sigma})$ denotes the PDF of $\mathbf{y}_k$ following the multivariate Gaussian distribution with expectation $\mathbf{W}\boldsymbol{\phi}_k$ and covariance matrix $\boldsymbol{\Sigma}$. The conditional PDF in equation (2) is the likelihood function of $\mathbf{Y}$ for parameters $\mathbf{W}$ and $\boldsymbol{\Sigma}$. According to the Bayes theorem, the PDF of $\mathbf{W}$ and $\boldsymbol{\Sigma}$ conditioned by $\mathbf{Y}$ is given as
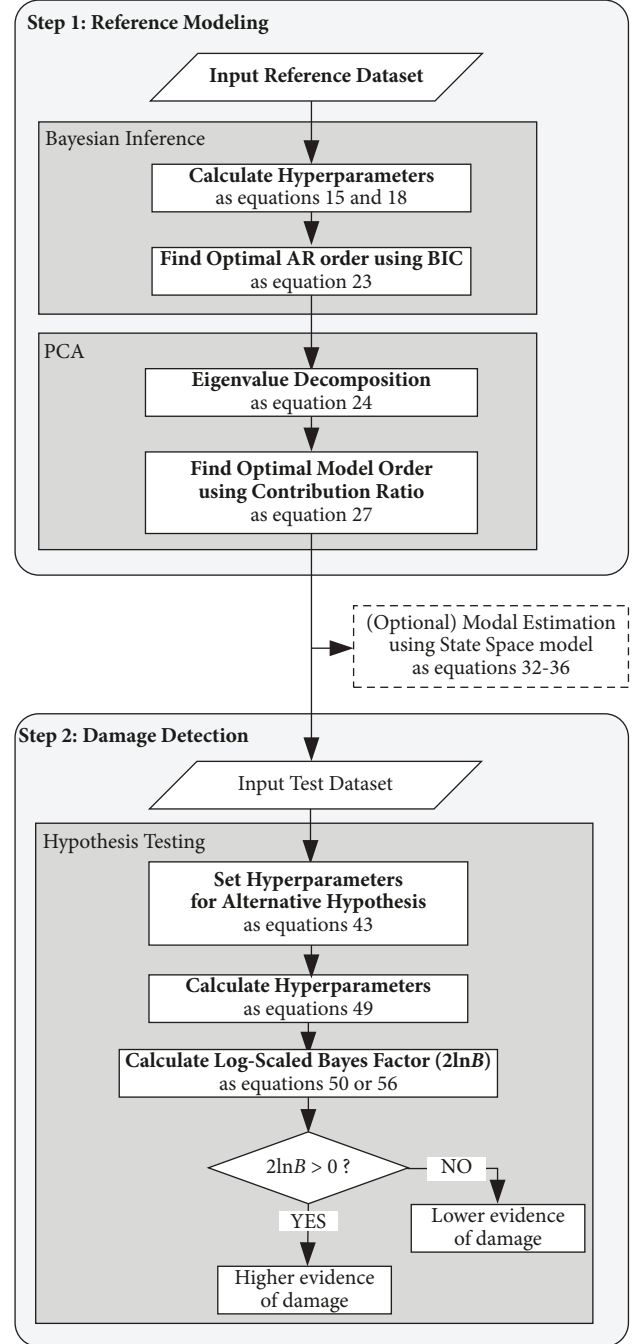
Figure 1: Outline of the proposed method.

$$p(\mathbf{W}, \boldsymbol{\Sigma} \mid \mathbf{Y}) = p(\mathbf{Y} \mid \mathbf{W}, \boldsymbol{\Sigma})p(\mathbf{W}, \boldsymbol{\Sigma})p(\mathbf{Y})^{-1}, \quad (3)$$

where $p(\mathbf{W}, \boldsymbol{\Sigma})$ and $p(\mathbf{W}, \boldsymbol{\Sigma} \mid \mathbf{Y})$ represent the prior and posterior PDF of $\mathbf{W}$ and $\boldsymbol{\Sigma}$, respectively; $p(\mathbf{Y})$ is a constant given as the marginal likelihood of $\mathbf{Y}$.

For Bayesian inference, this study adopts conjugate priors [22], which produce posterior distributions with invariant functional forms. The conjugate priors have an advantage for fast computation because they do not require MCMC. For a linear regressive model, the conjugate prior

for $\mathbf{W}$ and $\boldsymbol{\Sigma}$ is given as the following matrix-normal inverse-Wishart distribution [30].

$$\mathrm{p}(\mathbf{W}, \boldsymbol{\Sigma}) = \mathscr{MN}\left(\mathbf{W} \mid \mathbf{M}, \boldsymbol{\Sigma}, \mathbf{L}^{-1}\right)\mathscr{IW}\left(\boldsymbol{\Sigma} \mid \boldsymbol{\Psi}, \nu\right). \tag{4}$$

Therein, $\mathscr{MN}\left(\mathbf{W} \mid \mathbf{M}, \boldsymbol{\Sigma}, \mathbf{L}^{-1}\right)$ and $\mathscr{IW}\left(\boldsymbol{\Sigma} \mid \boldsymbol{\Psi}, \nu\right)$ stand, respectively, for the matrix-normal and inverse-Wishart distributions as

$$\mathscr{MN}\left(\mathbf{W} \mid \mathbf{M}, \boldsymbol{\Sigma}, \mathbf{L}^{-1}\right) = (2\pi)^{-\left(m^2 p/2\right)}\left|\mathbf{L}^{-1}\right|^{-(m/2)}|\boldsymbol{\Sigma}|^{-(mp/2)} \exp\left\{-\frac{1}{2}\mathrm{tr}\left[\mathbf{L}(\mathbf{W} - \mathbf{M})^{\mathrm{T}}\boldsymbol{\Sigma}^{-1}(\mathbf{W} - \mathbf{M})\right]\right\},$$

$$\mathscr{IW}\left(\boldsymbol{\Sigma} \mid \boldsymbol{\Psi}, \nu\right) = 2^{-(\nu m/2)}\Gamma_m\left(\frac{\nu}{2}\right)|\boldsymbol{\Psi}|^{(\nu/2)}|\boldsymbol{\Sigma}|^{-(\nu+m+1)/2}\exp\left\{-\frac{1}{2}\mathrm{tr}\left[\boldsymbol{\Psi}\boldsymbol{\Sigma}^{-1}\right]\right\}, \tag{5}$$

where $\mathrm{tr}[\cdot]$ represents the trace of a matrix, $|\cdot|$ denotes the determinant of a matrix, and $\Gamma_m(\cdot)$ is the multivariate gamma function. $\mathbf{M} \in \mathbb{R}^{m \times mp}$, $\mathbf{L} \in \mathbb{R}^{mp \times mp}$, $\boldsymbol{\Psi} \in \mathbb{R}^{m \times m}$, and $\nu \in \mathbb{R}$ are hyperparameters, i.e., the parameters which determine the functional form of the PDF for the parameters $\mathbf{W}$ and $\boldsymbol{\Sigma}$. Equations (2)–(4) engender the following posterior distribution [30].

$$\mathrm{p}(\mathbf{W}, \boldsymbol{\Sigma} \mid \mathbf{Y}) = \mathscr{MN}\left(\mathbf{W} \mid \mathbf{M}', \boldsymbol{\Sigma}, \mathbf{L}'^{-1}\right)\mathscr{IW}\left(\boldsymbol{\Sigma} \mid \boldsymbol{\Psi}', \nu'\right). \tag{6}$$

In equation (6), each hyperparameter is given as follows:

$$\mathbf{L}' = \mathbf{L} + \sum_{k=p+1}^{n} \boldsymbol{\phi}_k \boldsymbol{\phi}_k^{\mathrm{T}}, \tag{7}$$

$$\mathbf{M}' = \left(\mathbf{ML} + \sum_{k=p+1}^{n} \mathbf{y}_k \boldsymbol{\phi}_k^{\mathrm{T}}\right)\mathbf{L}'^{-1}, \tag{8}$$

$$\nu' = \nu + n - p, \tag{9}$$

$$\boldsymbol{\Psi}' = \boldsymbol{\Psi} + \sum_{k=p+1}^{n} \mathbf{y}_k \mathbf{y}_k^{\mathrm{T}} + \mathbf{MLM}^{\mathrm{T}} - \mathbf{M}'\mathbf{L}'\mathbf{M}'^{\mathrm{T}}. \tag{10}$$

Equations (2)–(4) and (6) lead the following marginal likelihood.

$$\mathrm{p}(\mathbf{Y}) \propto \frac{\Gamma_m\left(\nu'/2\right)}{\Gamma_m(\nu/2)}\frac{|\mathbf{L}|^{m/2}}{\left|\mathbf{L}'\right|^{m/2}}\frac{|\boldsymbol{\Psi}|^{\nu/2}}{\left|\boldsymbol{\Psi}'\right|^{\nu'/2}}. \tag{11}$$

Herein, $\propto$ represents that the right-hand side is proportional to the left-hand side.

2.2. Bayesian Inference for the Reference Dataset.

Let l sets of time series of acceleration be acquired as the reference dataset: $\mathbf{Y}_i = [\mathbf{y}_1^{i\mathrm{T}}, \ldots, \mathbf{y}_{n_i}^{i\mathrm{T}}]^{\mathrm{T}} (i = 1 \ldots l)$ stands for each of the time series where n_i $(i = 1 \ldots l)$ is its data length. Let $\mathscr{D}_{\mathrm{r}}$ represent the reference dataset as $\mathscr{D}_{\mathrm{r}} = \{\mathbf{Y}_1 \ldots \mathbf{Y}_l\}$, where the subscript "r" denotes "reference." Before observing the

reference dataset, we do not have any information about the value of the model parameters. Therefore, it is reasonable to adopt a so-called noninformative prior [22, 43], which represents unknown initial knowledge about the parameters. In equations (7)–(10), this study applies hyperparameters $[\mathbf{L}]_{ij} = 0 \ (i, j = 1 \ldots mp), \nu = 0,$ and $[\boldsymbol{\Psi}]_{ij} = 0 \ (i, j = 1 \ldots m)$ to represent the noninformative prior. As far as the abovementioned hyperparameters are adopted, the value of $\mathbf{M}$ does not alter the following calculation. The proposed noninformative prior and equations (7)–(10) generate the following posterior distribution:

$$\mathrm{p}(\mathbf{W}, \boldsymbol{\Sigma} \mid \mathscr{D}_{\mathrm{r}}) = \mathscr{MN}\left(\mathbf{W} \mid \mathbf{M}_{\mathrm{r}}, \boldsymbol{\Sigma}, \mathbf{L}_{\mathrm{r}}^{-1}\right)\mathscr{IW}\left(\boldsymbol{\Sigma} \mid \boldsymbol{\Psi}_{\mathrm{r}}, \nu_{\mathrm{r}}\right). \tag{12}$$

In equation (12), each hyperparameter is calculated as

$$\mathbf{L}_{\mathrm{r}} = \sum_{i=1}^{l} \sum_{k=p+1}^{n_i} \boldsymbol{\phi}_k^i \boldsymbol{\phi}_k^{i\mathrm{T}}, \tag{13}$$

$$\mathbf{M}_{\mathrm{r}} = \left(\sum_{i=1}^{l} \sum_{k=p+1}^{n_i} \mathbf{y}_k^i \boldsymbol{\phi}_k^{i\mathrm{T}}\right)\mathbf{L}_{\mathrm{r}}^{-1}, \tag{14}$$

$$\nu_{\mathrm{r}} = \sum_{i=1}^{l} \left(n_i - p\right), \tag{15}$$

$$\boldsymbol{\Psi}_{\mathrm{r}} = \sum_{i=1}^{l} \sum_{k=p+1}^{n_i} \mathbf{y}_k^i \mathbf{y}_k^{i\mathrm{T}} - \mathbf{M}_{\mathrm{r}}\mathbf{L}_{\mathrm{r}}\mathbf{M}_{\mathrm{r}}^{\mathrm{T}}, \tag{16}$$

where $\boldsymbol{\phi}_k^i = [\mathbf{y}_{k-p}^{i\mathrm{T}}, \ldots, \mathbf{y}_{k-1}^{i\mathrm{T}}]^{\mathrm{T}}$. The posterior distribution in equation (12) represents the updated knowledge after measuring the reference dataset and quantifies the uncertainty for each regressive parameter based on the observation. The time series in the reference dataset directly produce the hyperparameters in equations (13)–(16). The summations in equations (13), (14), and (16) are approximated with the following autocorrelation for fast computation:

$$\mathbf{R}(s) = \begin{cases} \dfrac{1}{N}\sum_{i=1}^{l}\sum_{k=s+1}^{n_i}\left(\mathbf{y}_k^i \mathbf{y}_{k-s}^{i\mathrm{T}}\right), & (\text{for } s \geq 0), \\ \\ \mathbf{R}(s)^{\mathrm{T}}, & (\text{for } s < 0). \end{cases} \tag{17}$$

Herein, N represents the total data length of the reference dataset, i.e., $N = \Sigma_{i=1}^{l} n_i$. Equations (13), (14), and (16) are approximated using autocorrelation functions, as shown in the following equations:

$$
\begin{aligned}
\mathbf{L}_r &= \sum_{i=1}^{l} \sum_{k=p+1}^{n_i} \begin{bmatrix} \mathbf{y}_{k-p}^{i} \\ \vdots \\ \mathbf{y}_{k-1}^{i} \end{bmatrix} \begin{bmatrix} \mathbf{y}_{k-p}^{i} \\ \vdots \\ \mathbf{y}_{k-1}^{i} \end{bmatrix}^{\mathrm{T}} \approx (N - pl) \begin{bmatrix} \mathbf{R}(0) & ,\ldots, & \mathbf{R}(1-p) \\ \vdots & \ddots & \vdots \\ \mathbf{R}(p-1) & ,\ldots, & \mathbf{R}(0) \end{bmatrix}, \\
\mathbf{M}_r &= \left(\sum_{i=1}^{l} \sum_{k=p+1}^{n_i} \mathbf{y}_{k}^{i} \begin{bmatrix} \mathbf{y}_{k-p}^{i} \\ \vdots \\ \mathbf{y}_{k-1}^{i} \end{bmatrix}^{\mathrm{T}} \right) \mathbf{L}_r^{-1} \approx [\mathbf{R}(p) \ldots \mathbf{R}(1)] \begin{bmatrix} \mathbf{R}(0) & ,\ldots, & \mathbf{R}(1-p) \\ \vdots & \ddots & \vdots \\ \mathbf{R}(p-1) & ,\ldots, & \mathbf{R}(0) \end{bmatrix}^{-1}, \\
\mathbf{\Psi}_r &\approx (N - pl)\mathbf{R}(0) - \mathbf{M}_r \mathbf{L}_r \mathbf{M}_r^{\mathrm{T}}.
\end{aligned}
\tag{18}
$$

To find appropriate AR order p, the following BIC [22, 38] is adopted.

$$
\begin{aligned}
\mathrm{BIC} = &-2\ln \mathrm{p}\left(\mathscr{D}_r \,|\, \widehat{\mathbf{W}}_r, \widehat{\mathbf{\Sigma}}_r \right) \\
&+ \left(m^2 p + \frac{m(m+1)}{2} \right) \ln\left(\Sigma_{i=1}^{l} \left(n_i - p \right) \right).
\end{aligned}
\tag{19}
$$

Therein, $\widehat{\mathbf{W}}_r$ and $\widehat{\mathbf{\Sigma}}_r$ are the most likelihood estimators (MLEs) of $\mathbf{W}$ and $\mathbf{\Sigma}$ for the reference dataset. The most likelihood estimators can be rewritten using the hyperparameters as

$$
\widehat{\mathbf{W}}_r = \left(\sum_{i=1}^{l} \sum_{k=p+1}^{n_i} \mathbf{y}_{k}^{i} \boldsymbol{\phi}_{k}^{i}{}^{\mathrm{T}} \right) \left(\sum_{i=1}^{l} \sum_{k=p+1}^{n_i} \boldsymbol{\phi}_{k}^{i} \boldsymbol{\phi}_{k}^{i}{}^{\mathrm{T}} \right)^{-1} = \mathbf{M}_r,
\tag{20}
$$

$$
\widehat{\mathbf{\Sigma}}_r = \frac{\sum_{i=1}^{l} \sum_{k=p+1}^{n_i} \left(\mathbf{y}_{k}^{i} - \widehat{\mathbf{W}}_r \boldsymbol{\phi}_{k}^{i} \right) \left(\mathbf{y}_{k}^{i} - \widehat{\mathbf{W}}_r \boldsymbol{\phi}_{k}^{i} \right)^{\mathrm{T}}}{\sum_{i=1}^{l} \left(n_i - p \right)} = \frac{\mathbf{\Psi}_r}{\nu_r}.
\tag{21}
$$

According to the well-known nature of the Gaussian model, $\ln \mathrm{p}(\mathscr{D}_r \,|\, \widehat{\mathbf{W}}_r, \widehat{\mathbf{\Sigma}}_r)$ in equation (19) is given as presented in the following equation:

$$
\ln \mathrm{p}\left(\mathscr{D}_r \,|\, \widehat{\mathbf{W}}_r, \widehat{\mathbf{\Sigma}}_r \right) = -\frac{\Sigma_{i=1}^{l} \left(n_i - p \right)}{2} \ln \left| \widehat{\mathbf{\Sigma}}_r \right| + \mathrm{Const}.
\tag{22}
$$

Using the hyperparameters and ignoring the constant, BIC in equation (19) is rewritten as

$$
\mathrm{BIC} = \nu_r \ln \left| \frac{\mathbf{\Psi}_r}{\nu_r} \right| + \left(m^2 p + \frac{m(m+1)}{2} \right) \ln \nu_r.
\tag{23}
$$

The AR order providing the lower BIC represents the better regressive model representing the reference dataset. Accordingly, the optimal AR order is automatically calculated from the reference dataset.

2.3. Principal Component Analysis. The posterior distribution for $\mathbf{W}$ is transformed into independent parameters for further analysis. For the PDF given in equation (12), the orthogonal basis for the transformation is obtained from the eigenvalue decomposition of the hyperparameter $\mathbf{L}_r$ as

$$
\mathbf{L}_r = \mathbf{U}\mathbf{\Lambda}\mathbf{U}^{\mathrm{T}} = [\mathbf{u}_1, \ldots, \mathbf{u}_{mp}] \mathrm{diag}[\lambda_1, \ldots, \lambda_{mp}] [\mathbf{u}_1, \ldots, \mathbf{u}_{mp}]^{\mathrm{T}},
\tag{24}
$$

where $\mathbf{\Lambda} \in \mathbb{R}^{mp \times mp}$ is the diagonal matrix consisting of the eigenvalues; $\mathbf{U} \in \mathbb{R}^{mp \times mp}$ is the orthogonal matrix consisting of the eigenvectors; $\mathrm{diag}[\lambda_1, \ldots, \lambda_{mp}]$ stands for the diagonal matrix consisting of the diagonal elements $\lambda_1, \ldots, \lambda_{mp}$. $\mathbf{u}_i$ and λ_i stand, respectively, for the i-th column of $\mathbf{U}$ and the i-th diagonal member of $\mathbf{\Lambda}$. For simplicity, let the eigenvalues be in descending order, i.e., $\lambda_1 > \ldots > \lambda_{mp}$. The orthogonal basis $\{ \mathbf{u}_1 \ldots \mathbf{u}_{mp} \}$ transforms the posterior distribution for $\mathbf{W}$ as follows: Letting $\widetilde{\mathbf{W}} = \mathbf{W}\mathbf{U}$ and $\widetilde{\mathbf{w}}_i = \mathbf{W}\mathbf{u}_i$ $(i = 1 \ldots mp)$, the PDF in equation (12) is transformed as

$$
\mathrm{p}\left(\widetilde{\mathbf{W}}, \mathbf{\Sigma} | \mathscr{D}_r \right) = \mathscr{M}\mathscr{N}\left(\widetilde{\mathbf{W}} | \widetilde{\mathbf{M}}, \mathbf{\Sigma}, \mathbf{\Lambda}^{-1} \right) \mathscr{I}\mathscr{W}\left(\mathbf{\Sigma} | \mathbf{\Psi}_r, \nu_r \right) = \prod_{i=1}^{mp} \left(\widetilde{\mathbf{w}}_i | \widetilde{\mathbf{m}}_i, \lambda_i^{-1} \mathbf{\Sigma} \right) \mathscr{I}\mathscr{W}\left(\mathbf{\Sigma} \,|\, \mathbf{\Psi}_r, \nu_r \right),
\tag{25}
$$

where $\widetilde{\mathbf{M}} = \mathbf{M}_r \mathbf{U}$ and $\widetilde{\mathbf{m}}_i = \mathbf{M}_r \mathbf{u}_i$ ($i = 1 \ldots mp$). Equation (25) shows that each vector $\widetilde{\mathbf{w}}_i$ is independent of the others.

The transformation described previously is comparable to the PCA of the vector $\boldsymbol{\phi}_k$. That is because equation (13) relates the abovementioned orthogonal basis and the covariance matrix of the vector $\boldsymbol{\phi}_k$ as follows:

$$\mathrm{cov}(\boldsymbol{\phi}_k) = \frac{\left(\sum_{i=1}^{l} \sum_{k=p+1}^{n_i} \boldsymbol{\phi}_k^i \boldsymbol{\phi}_k^i{}^{\mathrm{T}}\right)}{\left(\sum_{i=1}^{l}(n_i - p)\right)} \propto \mathbf{L}_r = \mathbf{U}\boldsymbol{\Lambda}\mathbf{U}^{\mathrm{T}}. \quad (26)$$

This equation demonstrates that the vectors $\mathbf{u}_1 \ldots \mathbf{u}_{mp}$ are the eigenvectors of the covariance matrix of $\boldsymbol{\phi}_k$. Therefore, the i-th principal components of $\boldsymbol{\phi}_k$ are given as $\mathbf{u}_i^{\mathrm{T}} \boldsymbol{\phi}_k$. According to the PCA theory, vector $\boldsymbol{\phi}_k$ is approximated with the first several principal components. The following contribution ratio is used widely to evaluate how principal components contribute to the approximation.

$$\mathrm{CR}(i) = \frac{\lambda_i}{\left(\sum_{j=1}^{mp} \lambda_j\right)}. \quad (27)$$

The abovementioned contribution ratio is applied to distinguish the damage-sensitive parameters from the other parameters.

The following steady state-space model is examined to clarify the relationship between modal properties and the PCA.

$$\mathbf{x}_{k+1} = \mathbf{A}\mathbf{x}_k + \mathbf{B}\mathbf{e}_k, \quad (28)$$

$$\mathbf{y}_k = \mathbf{C}\mathbf{x}_k + \mathbf{e}_k. \quad (29)$$

Here, $\mathbf{x}_k$ is a state vector representing structural response, and matrices $\mathbf{A}$, $\mathbf{B}$, and $\mathbf{C}$ are constant matrices. The modal frequencies, damping ratios, and mode shapes are estimated from matrices $\mathbf{A}$ and $\mathbf{C}$. As discussed in Appendix A, the eigensystem realization algorithm (ERA) [40] produces the estimators of $\mathbf{A}$ and $\mathbf{C}$ as

$$\mathbf{A} = \begin{bmatrix} \mathbf{u}_1 & , \ldots, & \mathbf{u}_q \end{bmatrix}^{\mathrm{T}} \begin{bmatrix} \mathbf{u}_{1[m+1:mp]} & , \ldots, & \mathbf{u}_{q[m+1:mp]} \\ \widetilde{\mathbf{w}}_1 & , \ldots, & \widetilde{\mathbf{w}}_q \end{bmatrix}, \quad (30)$$

$$\mathbf{C} = \begin{bmatrix} \mathbf{u}_{1[1:m]} & , \ldots, & \mathbf{u}_{q[1:m]} \end{bmatrix}. \quad (31)$$

In those equations, $\mathbf{u}_{i[a:b]}$ represents a vector that consists of the a-th to b-th elements of $\mathbf{u}_i$.

For the reference dataset, the modal properties are estimated by substituting the MLE given in equation (20) to $\mathbf{A}$. The MLE of matrix $\mathbf{A}$ is given as

$$\widehat{\mathbf{A}} = \begin{bmatrix} \mathbf{u}_1 & , \ldots, & \mathbf{u}_q \end{bmatrix}^{\mathrm{T}} \begin{bmatrix} \mathbf{u}_{1[m+1:mp]} & , \ldots, & \mathbf{u}_{q[m+1:mp]} \\ \widetilde{\mathbf{m}}_1 & , \ldots, & \widetilde{\mathbf{m}}_q \end{bmatrix}. \quad (32)$$

Modal properties are estimated with eigenvalue analysis of matrix $\widehat{\mathbf{A}}$ as

$$\left(\widehat{\mathbf{A}} - \lambda_{\mathrm{A}}\right)\boldsymbol{\psi} = 0, \quad (33)$$

where λ_{A} is one of the eigenvalues of $\widehat{\mathbf{A}}$ and $\boldsymbol{\psi}$ is the corresponding eigenvector. The angular frequency ω, damping ratio ξ, and the mode shape $\mathbf{s}$ are given as follows:

$$\omega = \frac{|(\ln \lambda_A)|}{\Delta t}, \quad (34)$$

$$\xi = -\cos \angle (\ln \lambda_A), \quad (35)$$

$$\mathbf{s} = \mathrm{real}\left(\begin{bmatrix} \mathbf{u}_{1[1:m]} & , \ldots, & \mathbf{u}_{q[1:m]} \end{bmatrix} \boldsymbol{\psi}\right), \quad (36)$$

where $\mathrm{abs}|(\cdot)|$, $\mathrm{real}(\cdot)$, and $\angle(\cdot)$ represent the absolute value, real part, and phase angle, respectively; Δt stands for the sampling interval.

Equations (30) and (31) show that the AR coefficients relate with the modal properties only on the vector space consisting of the orthogonal basis $\{\mathbf{u}_1 \ldots \mathbf{u}_q\}$. Namely, only q vectors $\widetilde{\mathbf{w}}_1 \ldots \widetilde{\mathbf{w}}_q$ represent the modal properties, and the other vectors $\widetilde{\mathbf{w}}_{q+1}, \ldots, \widetilde{\mathbf{w}}_{mp}$ are less relevant to them. The orthogonal transformation consequently separates physically meaningful and meaningless parameters. This study refers to the vectors $\widetilde{\mathbf{w}}_1 \ldots \widetilde{\mathbf{w}}_q$ as the damage-sensitive parameters. Let the damage-sensitive parameters and the other parameters be gathered in matrices, respectively, as $\widetilde{\mathbf{W}}_1 = [\widetilde{\mathbf{w}}_1, \ldots, \widetilde{\mathbf{w}}_q] \in \mathbb{R}^{mp \times q}$ and $\widetilde{\mathbf{W}}_2 = [\widetilde{\mathbf{w}}_{q+1}, \ldots, \widetilde{\mathbf{w}}_{mp}] \in \mathbb{R}^{mp \times (mp-q)}$. Equation (25) produces the following PDFs for $\widetilde{\mathbf{W}}_1$, $\widetilde{\mathbf{W}}_2$, and $\boldsymbol{\Sigma}$.

$$\mathrm{p}\left(\widetilde{\mathbf{W}}_1 \mid \boldsymbol{\Sigma}, \mathscr{D}_r\right) = \prod_{i=1}^{q} \mathscr{N}\left(\widetilde{\mathbf{w}}_i \mid \widetilde{\mathbf{m}}_i, \lambda_i^{-1}\boldsymbol{\Sigma}\right), \quad (37)$$

$$\mathrm{p}\left(\widetilde{\mathbf{W}}_2 \mid \boldsymbol{\Sigma}, \mathscr{D}_r\right) = \prod_{i=q+1}^{mp} \mathscr{N}\left(\widetilde{\mathbf{w}}_i \mid \widetilde{\mathbf{m}}_i, \lambda_i^{-1}\boldsymbol{\Sigma}\right), \quad (38)$$

$$\mathrm{p}\left(\boldsymbol{\Sigma} \mid \mathscr{D}_r\right) = \mathscr{IW}\left(\boldsymbol{\Sigma} \mid \boldsymbol{\Psi}_r, \nu_r\right). \quad (39)$$

3. Damage Detection

3.1. Hypothesis Testing. Bayesian hypothesis testing provides a framework to compare two competing statistical models representing the observed data [27]. This study adopts two statistical models, respectively, representing the healthy and damaged bridge. Following the hypothesis testing precedent, the healthy and damaged bridge models are designated as the "null hypothesis" and the "alternative hypothesis."

Let $\mathscr{D}_t$ denote the test dataset for the hypothesis testing. Herein, subscript "t" stands for "test." Let $\widetilde{\mathbf{W}}_1^r$ and $\widetilde{\mathbf{W}}_1^t$ represent the damage-sensitive parameters for the reference and test datasets, respectively. This study formulates the hypotheses according to the following conditions:

(i) The damage-sensitive parameters for the null hypothesis $\mathscr{H}_0$ are consistent between the reference and test datasets, i.e., $\widetilde{\mathbf{W}}_1^r = \widetilde{\mathbf{W}}_1^t$

(ii) The damage-sensitive parameters for the alternative hypothesis $\mathscr{H}_1$ differ between the reference and test datasets, i.e., $\widetilde{\mathbf{W}}_1^{\mathrm{r}} \neq \widetilde{\mathbf{W}}_1^{\mathrm{t}}$

(iii) Parameters $\widetilde{\mathbf{W}}_2$ and $\mathbf{\Sigma}$ for both hypotheses are consistent between the reference and test datasets

$$\mathrm{p}(\mathbf{W},\mathbf{\Sigma}\,|\,\mathscr{H}_0) = \mathrm{p}(\mathbf{W},\mathbf{\Sigma}\,|\,\mathscr{D}_{\mathrm{r}}) = \mathscr{MN}(\mathbf{W}\,|\,\mathbf{M}_{\mathrm{r}},\mathbf{\Sigma},\mathbf{L}_{\mathrm{r}}^{-1})\mathscr{IW}(\mathbf{\Sigma}\,|\,\mathbf{\Psi}_{\mathrm{r}},\nu_{\mathrm{r}}). \tag{40}$$

Under the alternative hypothesis, damage-sensitive parameters $\widetilde{\mathbf{W}}_1^{\mathrm{t}}$ are altered from the reference dataset and unknown before observing the test dataset. Bayesian statistics represents the parameters with less knowledge as PDFs with broad variances. As shown in equation (37), each vector $\widetilde{\mathbf{w}}_i$ has variance $\lambda_i^{-1}\mathbf{\Sigma}$ in the posterior distribution. The eigenvalues of $\mathbf{L}_{\mathrm{r}}$ are usually large enough, i.e., $1 \ll \lambda_i\ (i=1,\ldots,q)$ because sufficient data length is available for the reference dataset. So, the alternative hypothesis adopts the following PDF with broad variances instead of equation (37):

$$p(\widetilde{\mathbf{W}}_1^{\mathrm{t}}\,|\,\mathbf{\Sigma},\mathscr{H}_1) = \prod_{i=1}^{q}\mathscr{N}(\widetilde{\mathbf{w}}_i\,|\,\mathbf{0},\mathbf{\Sigma}). \tag{41}$$

Here, 0 is adopted as the mean value of the damage-sensitive parameters $\widetilde{\mathbf{W}}_1^{\mathrm{t}}$ to avoid bias derived from the reference dataset.

Consequently, the PDF for parameters $\mathbf{W}$ and $\mathbf{\Sigma}$ are given as

$$\mathrm{p}(\mathbf{W},\mathbf{\Sigma}\,|\,\mathscr{H}_1) = \mathscr{MN}(\mathbf{W}\,|\,\mathbf{M}_{\mathrm{alt}},\mathbf{\Sigma},\mathbf{L}_{\mathrm{alt}}^{-1})\mathscr{IW}(\mathbf{\Sigma}|\mathbf{\Psi}_{\mathrm{r}},\nu_{\mathrm{r}}), \tag{42}$$

where

$$\begin{aligned}\mathbf{M}_{\mathrm{alt}} &= [\mathbf{0},\ldots,\mathbf{0}\,\widetilde{\mathbf{m}}_{q+1},\ldots,\widetilde{\mathbf{m}}_{mp}]\mathbf{U}^{\mathrm{T}},\\ \mathbf{L}_{\mathrm{alt}} &= \mathbf{U}\mathrm{diag}[1,\ldots,1,\lambda_{q+1},\ldots,\lambda_{mp}]\mathbf{U}^{\mathrm{T}}.\end{aligned} \tag{43}$$

Letting $\mathbf{M}_0 = \mathbf{M}_{\mathrm{r}}$, $\mathbf{L}_0 = \mathbf{L}_{\mathrm{r}}$, $\mathbf{M}_1 = \mathbf{M}_{\mathrm{alt}}$, and $\mathbf{L}_1 = \mathbf{L}_{\mathrm{alt}}$ for simplicity, the PDFs for the null and alternative hypotheses are presented as follows:

$$\mathrm{p}(\mathbf{W},\mathbf{\Sigma}\,|\,\mathscr{H}_\kappa) = \mathscr{MN}(\mathbf{W}\,|\,\mathbf{M}_\kappa,\mathbf{\Sigma},\mathbf{L}_\kappa^{-1})\mathscr{IW}(\mathbf{\Sigma}\,|\,\mathbf{\Psi}_{\mathrm{r}},\nu_{\mathrm{r}})\ (\kappa=0,1). \tag{44}$$

Using the PDF in equation (44), evidence functions of $\mathscr{D}_{\mathrm{t}}$ for the hypothesis testing are

$$\mathrm{p}(\mathscr{D}_{\mathrm{t}}\,|\,\mathscr{H}_\kappa) = \iint\mathrm{p}(\mathscr{D}_{\mathrm{t}}\,|\,\mathbf{W},\mathbf{\Sigma})\mathrm{p}(\mathbf{W},\mathbf{\Sigma}\,|\,\mathscr{H}_\kappa)\mathrm{d}\mathbf{W}\,\mathrm{d}\mathbf{\Sigma}\ (\kappa=0,1). \tag{45}$$

The only difference between the two hypotheses is the distribution of the damage-sensitive parameters $\widetilde{\mathbf{W}}_1^{\mathrm{t}}$ relevant to the modal properties. The uncertainty involved in the other parameters is marginalized and canceled out by the integration in equation (45).

The Bayes factor is the ratio of the two evidence functions shown as follows:

Under the null hypothesis, no parameter is altered between the reference and the test datasets. Therefore, the PDF of the parameters for the null hypothesis is identical to equation (12), i.e.,

$$B(\mathscr{D}_{\mathrm{t}}) = \frac{\mathrm{p}(\mathscr{D}_{\mathrm{t}}\,|\,\mathscr{H}_1)}{\mathrm{p}(\mathscr{D}_{\mathrm{t}}\,|\,\mathscr{H}_0)}. \tag{46}$$

According to the well-known scale as the likelihood ratio test statistics, Kass and Raftery [27] interpreted the Bayes factor on twice the natural logarithm scale as

$$2\ln B(\mathscr{D}_{\mathrm{t}}) = 2\ln\mathrm{p}(\mathscr{D}_{\mathrm{t}}\,|\,\mathscr{H}_1) - 2\ln\mathrm{p}(\mathscr{D}_{\mathrm{t}}\,|\,\mathscr{H}_0). \tag{47}$$

When the test dataset is in favor of the alternative hypothesis, its evidence function is higher against the null hypothesis, i.e., $\mathrm{p}(\mathscr{D}_{\mathrm{t}}\,|\,\mathscr{H}_1) > \mathrm{p}(\mathscr{D}_{\mathrm{t}}\,|\,\mathscr{H}_0)$. So, if the damage-sensitive parameters differ from the reference dataset, $2\ln B$ likely exceeds 0, and vice versa. Therefore, this study adopts $2\ln B = 0$ as the threshold for damage detection where the model evidence for the null and the alternative hypotheses are equivalent, i.e., $\mathrm{p}(\mathscr{D}_{\mathrm{t}}\,|\,\mathscr{H}_1) = \mathrm{p}(\mathscr{D}_{\mathrm{t}}\,|\,\mathscr{H}_0)$. Kass and Raftery [27] proposed the scale shown in Table 1. For example, if $2\ln B$ is greater than 10, the evidence against the null hypothesis is interpreted as "*very strong.*"

3.2. Global Damage Indicator. Let $\mathbf{Y}_{\mathrm{t}} = [\mathbf{y}_1^{\mathrm{tT}},\ldots,\mathbf{y}_{n_{\mathrm{t}}}^{\mathrm{tT}}]^{\mathrm{T}}$ represent a time series observed for hypothesis testing, where n_{t} stands for the data length. This section adopts the whole time series as the test dataset, i.e., $\mathscr{D}_{\mathrm{t}} = \mathbf{Y}_{\mathrm{t}}$. Equation (11) gives the following evidence function:

$$\mathrm{p}(\mathbf{Y}_{\mathrm{t}}\,|\,\mathscr{H}_\kappa) \propto \frac{\Gamma_m(\nu_{\mathrm{r}}'/2)}{\Gamma_m(\nu_{\mathrm{r}}/2)}\frac{|\mathbf{L}_\kappa|^{m/2}}{|\mathbf{L}_\kappa'|^{m/2}}\frac{|\mathbf{\Psi}_{\mathrm{r}}|^{\nu_{\mathrm{r}}/2}}{|\mathbf{\Psi}_\kappa'|^{\nu_{\mathrm{r}}'/2}}. \tag{48}$$

In equation (48), ν_{r}', $\mathbf{L}_\kappa$, and $\mathbf{\Psi}_\kappa'$ stand for the hyperparameters of the posterior distribution after test dataset observation, i.e., the hyperparameters of $\mathrm{p}(\mathbf{W},\mathbf{\Sigma}\,|\,\mathbf{Y}_{\mathrm{t}},\mathscr{H}_\kappa)$. The following equations calculate each hyperparameter:

$$\begin{aligned}\mathbf{L}_\kappa' &= \mathbf{L}_\kappa + \sum_{k=p+1}^{n_{\mathrm{t}}}\boldsymbol{\phi}_k^{\mathrm{t}}\boldsymbol{\phi}_k^{\mathrm{tT}},\\ \mathbf{M}_\kappa' &= \left(\mathbf{M}_\kappa\mathbf{L}_\kappa + \sum_{k=p+1}^{n_{\mathrm{t}}}\mathbf{y}_k^{\mathrm{t}}\boldsymbol{\phi}_k^{\mathrm{tT}}\right)\mathbf{L}_\kappa'-1,\\ \nu_{\mathrm{r}}' &= \nu_{\mathrm{r}} + n_{\mathrm{t}} - p,\\ \mathbf{\Psi}_\kappa' &= \mathbf{\Psi}_{\mathrm{r}} + \sum_{k=p+1}^{n_{\mathrm{t}}}\mathbf{y}_k^{\mathrm{t}}\mathbf{y}_k^{\mathrm{tT}} + \mathbf{M}_\kappa\mathbf{L}_\kappa\mathbf{M}_\kappa^{\mathrm{T}} - \mathbf{M}_\kappa'\mathbf{L}_\kappa'\mathbf{M}_\kappa'^{\mathrm{T}}.\end{aligned} \tag{49}$$

Here, $\boldsymbol{\phi}_k^{\mathrm{t}} = [\mathbf{y}_{k-1}^{\mathrm{tT}},\ldots,\mathbf{y}_{k-p}^{\mathrm{tT}}]^{\mathrm{T}}$. Accordingly, equation (48) gives the following log-scaled Bayes factor.

Table 1: Interpretation of Bayes factors [27].

$2 \ln B(\mathscr{D}_t)$	$B(\mathscr{D}_t)$	Evidence against $\mathscr{H}_0$
0 to 2	1 to 3	Not worth more than bare mention
2 to 6	3 to 20	Positive
6 to 10	20 to 150	Strong
>10	>150	Very strong

$$2 \ln B(\mathbf{Y}_t) = \nu_r' \left(\ln |\mathbf{\Psi}_0'| - \ln |\mathbf{\Psi}_1'| \right) + m \left(\ln |\mathbf{L}_0'| - \ln |\mathbf{L}_1'| \right) - m \sum_{k=1}^{q} \ln \lambda_k. \tag{50}$$

The log-scaled Bayes factor in equation (50) is designated as the "global Bayes factor" because it detects global changes in the modal response.

3.3. Local Damage Indicator.
The hypothesis testing to estimate the damage location is formulated as follows. Let $y_k^{(j)}$ stand for the j-th element of $\mathbf{y}_k^t$, and let $\mathbf{y}_k^{(-j)}$ stand for the vector except for the j-th element from $\mathbf{y}_k^t$. The time series of the j-th element $\mathbf{Y}_t^{(j)} = [y_1^{(j)}, \ldots, y_{n_t}^{(j)}]^T$ is adopted as the test dataset, i.e., $\mathscr{D}_t = \mathbf{Y}_t^{(j)}$. The likelihood for $y_k^{(j)}$ is transformed as follows, according to the Gaussian nature [22]:

$$p\left(y_k^{(j)} \mid \boldsymbol{\phi}_k, \mathbf{W}, \mathbf{\Sigma}\right) = \int \mathscr{N}\left(\mathbf{y}_k \mid \mathbf{W}\boldsymbol{\phi}_k, \mathbf{\Sigma}\right) d\mathbf{y}_k^{(-j)} = \mathscr{N}\left(y_k^{(j)} \mid \mathbf{W}^{(j)}\boldsymbol{\phi}_k, \sigma_j^2\right). \tag{51}$$

Therein, $\mathbf{W}^{(j)}$ stands for the j-th row of $\mathbf{W}$; σ_j^2 stands for the j-th diagonal element of $\mathbf{\Sigma}$. The likelihood function for $\mathbf{Y}_t^{(j)}$ satisfies the following relation:

$$p\left(\mathbf{Y}_t^{(j)} \mid \mathbf{W}^{(j)}, \sigma_j^2\right) \propto \prod_{k=p+1}^{n_t} \mathscr{N}\left(y_k^{(j)} \mid \mathbf{W}^{(j)}\boldsymbol{\phi}_k, \sigma_j^2\right). \tag{52}$$

Because the likelihood function only has parameters $\mathbf{W}^{(j)}$ and σ_j^2, the evidence function for hypothesis testing can be simplified as shown in the following equation:

$$p\left(\mathbf{Y}_t^{(j)} \mid \mathscr{H}_\kappa\right) = \iint p\left(\mathbf{Y}_t^{(j)} \mid \mathbf{W}^{(j)}, \sigma_j^2\right) p\left(\mathbf{W}^{(j)}, \sigma_j^2 \mid \mathscr{H}_\kappa\right) d\mathbf{W}^{(j)} d\left(\sigma_j^2\right) (\kappa = 0,1). \tag{53}$$

The PDF of $\mathbf{W}^{(j)}$ and σ_j^2 are approximately derived from equations (40) and (42) as

$$p\left(\mathbf{W}^{(j)}, \sigma_j^2 \mid \mathscr{H}_\kappa\right) = \mathscr{N}\left(\mathbf{W}^{(j)} \mid \mathbf{M}_\kappa^{(j)}, \sigma_j^2 \mathbf{L}_\kappa^{-1}\right) \mathscr{IW}\left(\sigma_j^2 \mid \psi_r^{(j)}, \nu_r\right) (\kappa = 0,1), \tag{54}$$

where $\mathbf{M}_\kappa^{(j)}$ and $\psi_r^{(j)}$ in equation (54) correspond, respectively, to the j-th row of $\mathbf{M}_\kappa$ and the j-th diagonal element of $\mathbf{\Psi}_r$. In a similar manner to that discussed in Section 2.1, the evidence functions in equation (53) are given as

$$p\left(\mathbf{Y}_t^{(j)} | \mathscr{H}_\kappa\right) \propto \frac{\Gamma_1(\nu'/2)}{\Gamma_1(\nu/2)} \frac{|\mathbf{L}_\kappa|^{1/2}}{|\mathbf{L}_\kappa'|^{1/2}} \frac{\left(\psi_r^{(j)}\right)^{\nu/2}}{\left(\psi_\kappa'^{(j)}\right)^{\nu'/2}} (\kappa = 0,1). \tag{55}$$

Here, $\psi_\kappa'^{(j)}$ stands for the j-th diagonal elements of the matrices $\mathbf{\Psi}_\kappa'$. The log-scaled Bayes factor is accordingly given as

$$2 \ln B\left(\mathbf{Y}_t^{(j)}\right) = \nu_r'\left(\ln \psi_0'^{(j)} - \ln \psi_1'^{(j)}\right)$$

$$+ \left(\ln |\mathbf{L}_0'| - \ln |\mathbf{L}_1'|\right) - \sum_{k=1}^{q} \ln \lambda_k. \tag{56}$$

The log-scaled Bayes factor given in equation (56) is designated as the "local Bayes factor."

4. Case Study

4.1. Target Bridge. This study provides a case study for a simply supported truss bridge to assess the feasibility of the proposed method. Field experiments were conducted on the bridge with a moving vehicle [41]. The bridge is a single-lane through-type steel Warren truss with 59.2 m span length, 8 m maximum height, and 3.6 m width, as presented in Figure 2. The vehicle used for the experiment is a two-axle recreational vehicle with a total weight of about 21 kN. During the investigation, all traffic except for the loading vehicle was prohibited. Eight uniaxial accelerometers were installed on the bridge deck to measure vertical vibrations, as presented in Figure 3. The sampling rate of each sensor was 200 Hz.

The truss members were severed in the field experiment. Figures 4(a) and 4(b) portray the schematic diagrams and photographs of the damaged members, respectively. The following five damage scenarios were considered: the INT scenario represents the intact bridge without damage. For the DMG1 scenario, half-cut damage was applied to the vertical truss member at midspan (the vertical member in a different color on the A3 sensor in Figure 3). For the DMG2 scenario, full-cut damage was applied to the same member. After that, the damaged member was repaired, designated as the RPD scenario. For the DMG3 scenario, a full cut was applied in a vertical member at 5/8th-span (the vertical member in a different color on the A4 sensor in Figure 3) after examining the RPD scenario. For the INT scenario, the vehicle passed over the deck at three speeds: 30 km/h, 40 km/h, and 50 km/h. For these analyses, INT30, INT40, and INT50 represent the scenarios at the three vehicle speeds. The vehicle passed only at 40 km/h for the other damage scenarios. Table 2 presents the vehicle loading scenarios. The damage experiment is motivated by the damage event for which a ruptured truss member was discovered during a bridge inspection in Japan [44]. More details of the field experiment and the data are available from the related data paper [41] and data repository [45]. We can also find the design dimensions for all the steel truss components and reinforced concrete slab in [41]. Another earlier study [11] investigated damage detection for this bridge based on modal identification.

Figures 5(a)–5(g) present the acceleration time series at sensor A3 for INT30, INT40, INT50, DMG1, DMG2, RPD, and DMG3, respectively. The linear trends in the time series were removed in advance. This case study adopts raw time series data with no preprocessing except for removing linear trends. As shown in Figures 5(a)–5(c), different vehicle speeds produce different transient responses of the bridge. The unsteady ambient loading can be a source of false alerts, as shown in Appendix B. In Figures 5(b), 5(d)–5(g), where vehicle speed was 40 km/h, the difference in the waveforms is not so significant. To examine changes in the modal response in the measured time series, the power spectral density (PSD) curve is widely used. Figure 6 portrays PSD curves from each time series, estimated as periodograms with the rectangular window. In the PSD

curves, several natural frequencies appear as peaks. Figure 6(a) shows that the dominant mode around 3 Hz slightly altered in DMG2, possibly because of the severed member at the midspan. The difference between INT40 and DMG1 is hard to distinguish in this figure. Figure 6(b) implies that the damage altered the higher modes, but the peaks are ambiguous at the higher frequency range compared to the dominant mode. Engineers can compare the frequencies for damage detection, but it is not always easy to distinguish changes by classical peak-picking. For instance, they need to choose the modal frequency for comparison. Preliminary calibration is required to set thresholds for peak-pick to automate damage detection. Also, they should estimate several samples from multiple measurements and compare them with a statistical approach because the frequencies involve estimation errors. Unsteady ambient loadings often make these procedures harder. Although they have more advanced ways, as discussed in Section 1.1, automating and generalizing damage detection procedures are still challenging.

4.2. Reference Modeling. All samples obtained from INT30, INT40, and INT50 were adopted as the reference dataset in this section. Figure 7 shows a plot of the BIC for the AR order. The vertical dashed line in Figure 7 depicts the optimal AR order $p = 94$. Accordingly, this study adopted $p = 94$ as the AR order. The PCA produces the contribution ratios shown in Figure 8. Here, the first and second principal components have a contribution ratio of around 30% and dominantly represent the vector ϕ_k. The third to tenth principal components have contribution ratios of about 5% to 2%; the others' contribution ratios are less than 1%. The first two principal components likely represent the dominant mode because it primarily contributes to the bridge vibration. The third to tenth principal components likely represent the other higher modes, whose modal responses are relatively small. This study applies the first to tenth principal components, i.e., $q = 10$.

With $q = 10$, the state-space model produces modal properties of five modes. Figures 9(a)–9(e) present the five mode shapes calculated by equation (36). Here, circles and squares in the diagram represent modal deformations, respectively, at A1 to A5 and A6 to A8 sensors. The frequency and damping ratios calculated by equations (34) and (35) are given in the captions of each figure. For Figures 9(a) and 9(b), we can identify the first and second bending modes. Although the estimated mode shapes in Figures 9(c)–9(e) are not evident enough because of the limitation of the number of measurement points, we can identify the corresponding modes by comparing them with a structural model. The frequencies and mode shapes correspond well with results from finite element analysis in an earlier study [11]. The earlier study indicates that the estimated modes are identical to the bridge's first to fifth bending modes. Accordingly, the damage-sensitive parameters in this case study are related to the first to fifth bending modal frequencies and mode shapes. Contrarily, the estimated damping ratios are much lower than physically expected. The possible reason is that the ERA
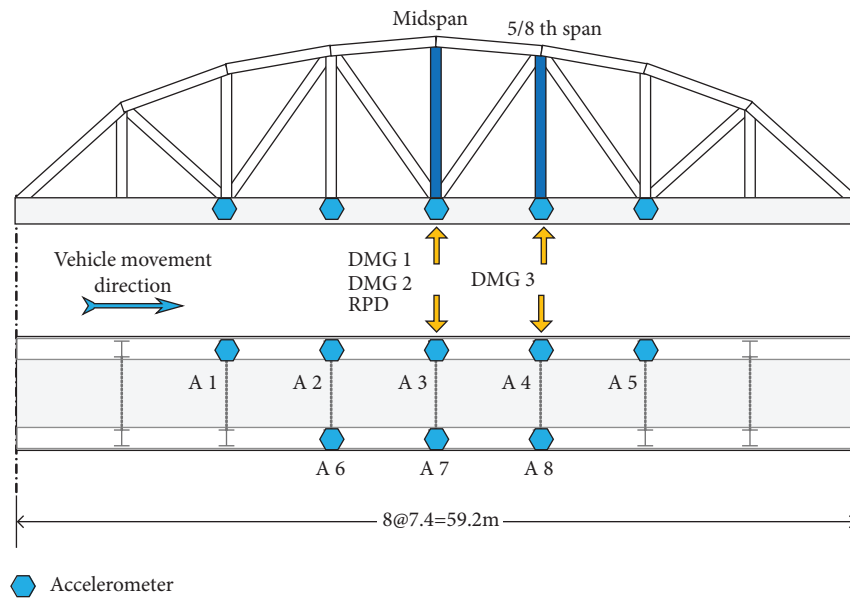
FIGURE 2: Photographs of the target bridge [41].

FIGURE 3: Sensor deployment and damage location [41].
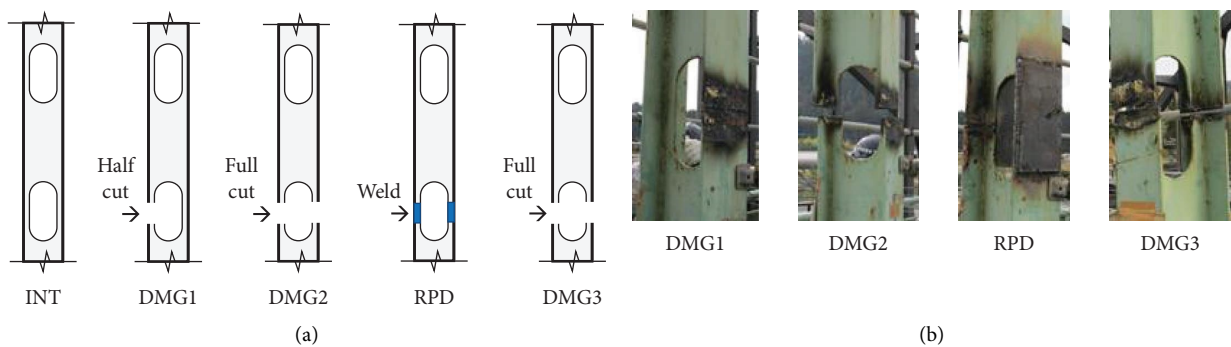

(a)

(b)

FIGURE 4: Damage scenarios: (a) schematic diagrams and (b) photographs of damaged members [41].

TABLE 2: Scenarios considered in the field experiment.

	Description	Vehicle speed (km/h)	Numbers of experiments
INT30	Intact bridge	30	11
INT40	Intact bridge	40	10
INT50	Intact bridge	50	5
DMG1	Half cut in vertical member at midspan	40	12
DMG2	Full cut in vertical member at midspan	40	10
RPD	Repair of the member at midspan	40	10
DMG3	Full cut in vertical member at 5/8th-span	40	10
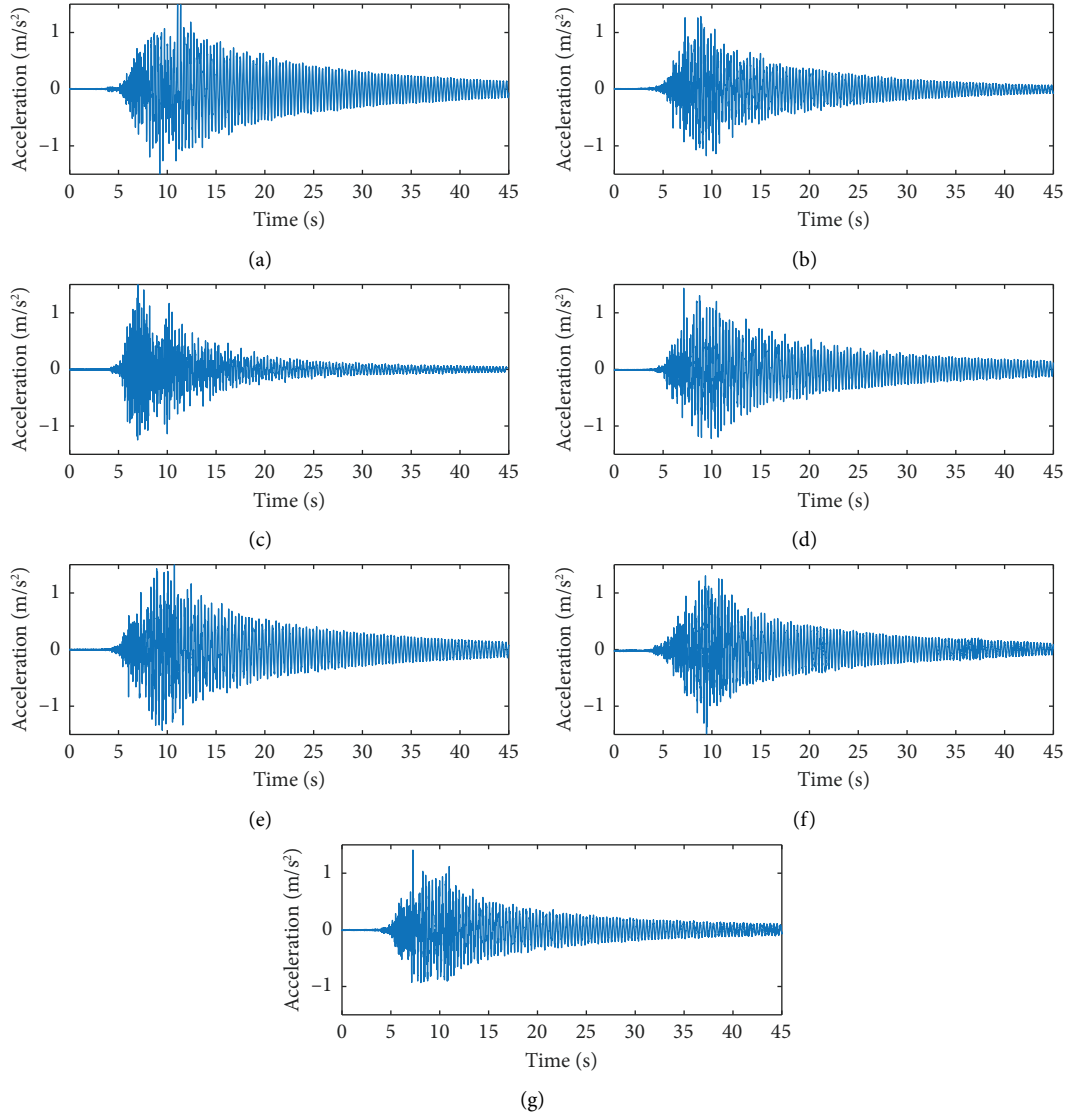
FIGURE 5: Measured time series of A3 sensor for (a) INT30, (b) INT40, (c) INT50, (d) DMG1, (e) DMG2, (f) RPD, and (g) DMG3.

assumes impulse response, whereas actual ambient loads produce continuous excitation.

4.3. Damage Detection. This case study adopts the INT as a reference scenario for DMG1 and DMG2 scenarios and the RPD scenario as a reference scenario for the DMG3 scenario because the modal properties changed after the repair of the damaged member. The following two cases are considered:

(i) Case 1: INT40 is adopted as a reference scenario for DMG1 and DMG2, but RPD is adopted as a reference scenario for DMG3

(ii) Case 2: INT30, INT40, and INT50 are adopted as a reference scenario for DMG1 and DMG2

Table 3 presents the conditions described above.

$2\ln B = 0$ is adopted as the threshold for damage detection, as mentioned in Section 3.1. The threshold is designated as a "critical value" for hypothesis testing. For the reference dataset, the leave-one-out cross-validation (CV) technique is applied to assess the validity of the Bayes factors: one of the time series (e.g., $\mathbf{Y}_1$) is taken out from this set as a test sample; then, the remaining samples $\{\mathbf{Y}_2, \ldots, \mathbf{Y}_l\}$ are referred as the reference dataset, i.e., $\mathcal{D}_r = \{\mathbf{Y}_2, \ldots, \mathbf{Y}_l\}$ and $\mathcal{D}_t = \mathbf{Y}_1$. Consequently, the l Bayes factors are obtained from the l samples from the reference dataset. The Bayes factors calculated using the CV technique are designated as "CV samples." The Bayes factor is validated as a robust anomaly indicator when CV samples are lower than the null hypothesis. On the other hand, if most of the CV samples are over the critical value, false positives are suspected (see also Appendix B).

Figures 10(a) and 10(b) present global Bayes factors for Cases 1 and 2, respectively. For INT and RPD scenarios, CV samples are shown in Figure 10. In addition, the critical value is depicted as a red horizontal line. Table 4 summarizes the mean values and the correct answer ratio of the global Bayes factors for each scenario. Here, Bayes factors meeting
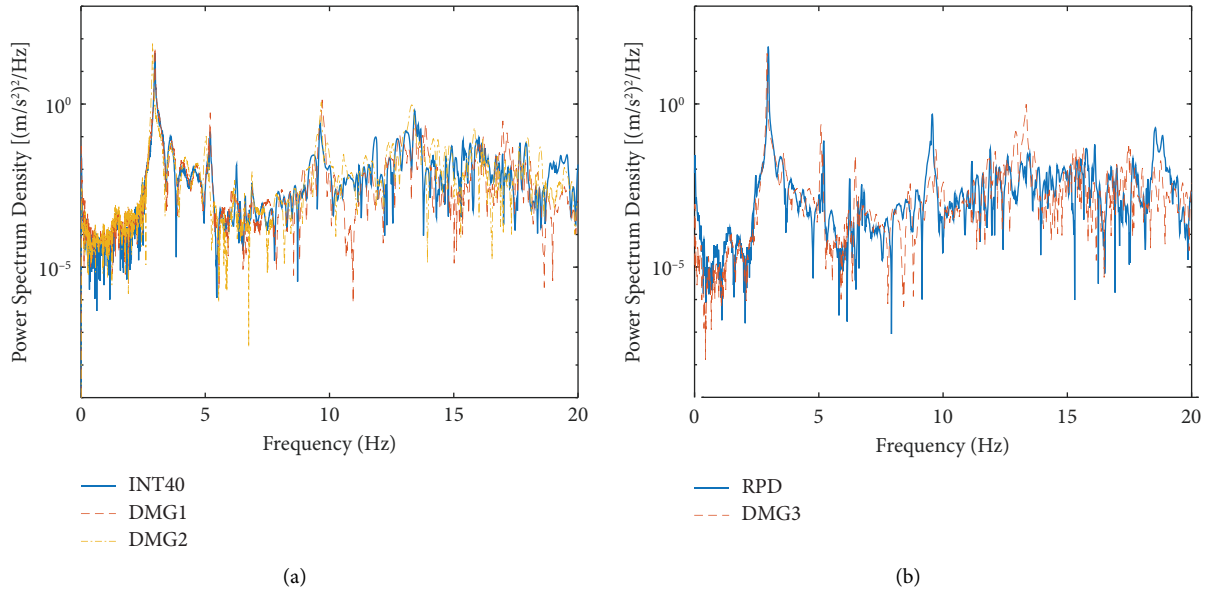
FIGURE 6: Measured PSD curves of A3 sensor: (a) for INT40, DMG1, and DMG2, (b) for RPD and DMG3.
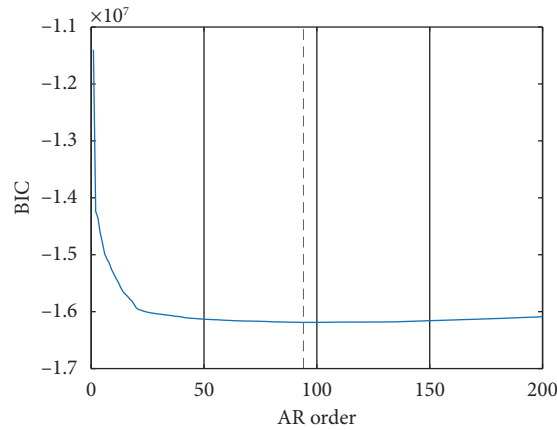

FIGURE 7: BIC with respect to the AR orders.
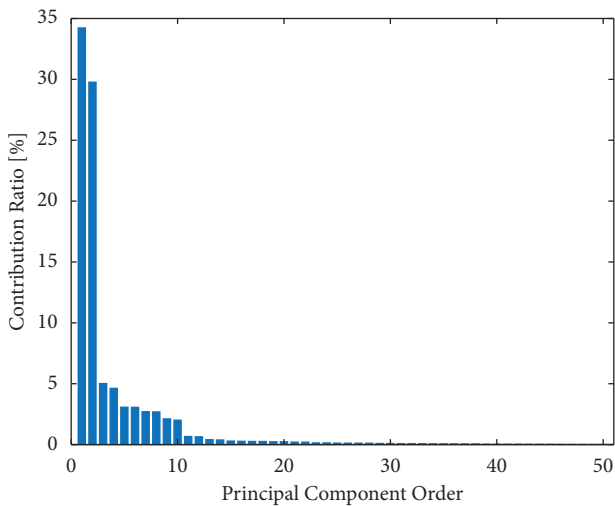

FIGURE 8: Contribution ratios.

$2\ln B < 0$ are correct answers for the CV samples; $2\ln B > 0$ are as correct answers for the damage scenarios. Except for DMG1, every global Bayes factor result in the correct answer. For DMG1, 10 out of 12 samples indicate the correct answer for both cases. According to the scale cited in Table 1, every damaged scenario, including DMG1, resulted in much higher Bayes factors than $2\ln B = 10$ in their mean value, which is "very strong" evidence for the alternative hypothesis against the null hypothesis. These results describe that the proposed Bayes factors are sensitive enough even to DMG1. Results for Case 2 demonstrate that the proposed method is sufficiently robust against unexpected bias caused by different vehicle speeds. Compared with Appendix B, these results indicate that the proposed method reduces false alerts caused by load-induced noise.

Figures 11(a) and 11(b) depict the local Bayes factors for Cases 1 and 2, respectively. Legends in the figures correspond to the measurement locations in Figure 3; CV samples

Freq. = 2.97 Hz, Damp. Ratio = 0.0077 %

(a)

Freq. = 6.87 Hz, Damp. Ratio = 0.015 %

(b)

Freq. = 9.59 Hz, Damp. Ratio = 0.027 %

(c)

Freq. = 10.5 Hz, Damp. Ratio = 0.033 %

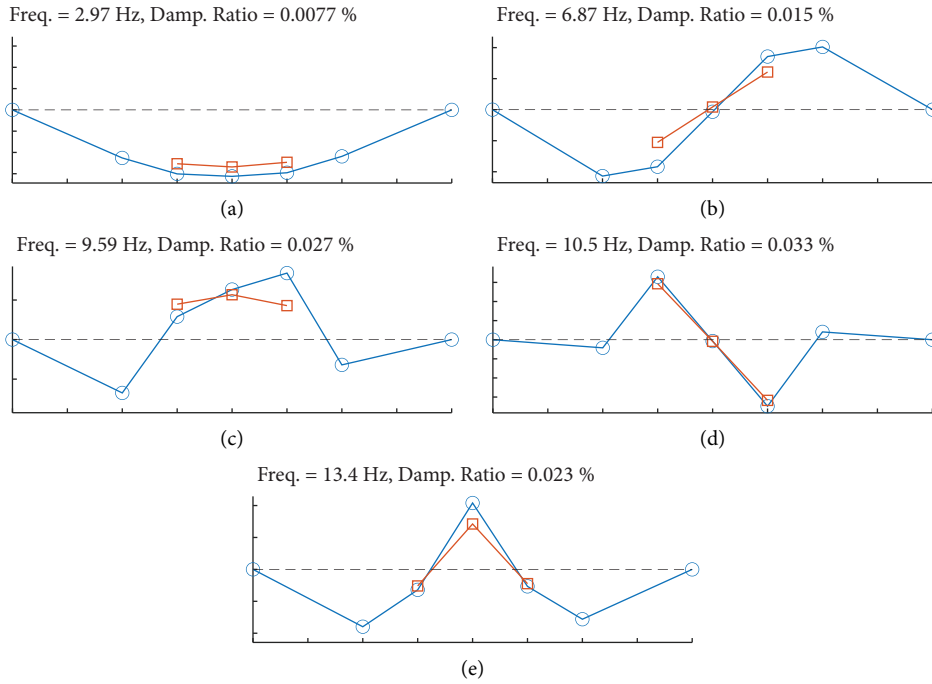(d)

Freq. = 13.4 Hz, Damp. Ratio = 0.023 %

(e)

FIGURE 9: Estimated modal properties: (a) 1st bending, (b) 2nd bending, (c) 3rd bending, (d) 4th bending, and (e) 5th bending.

TABLE 3: Cases considered for damage detection.

	Reference scenarios	Damage scenarios
Case 1	INT40	DMG1 and DMG2
	RPD	DMG3
Case 2	INT30, INT40, and INT50	DMG1 and DMG2
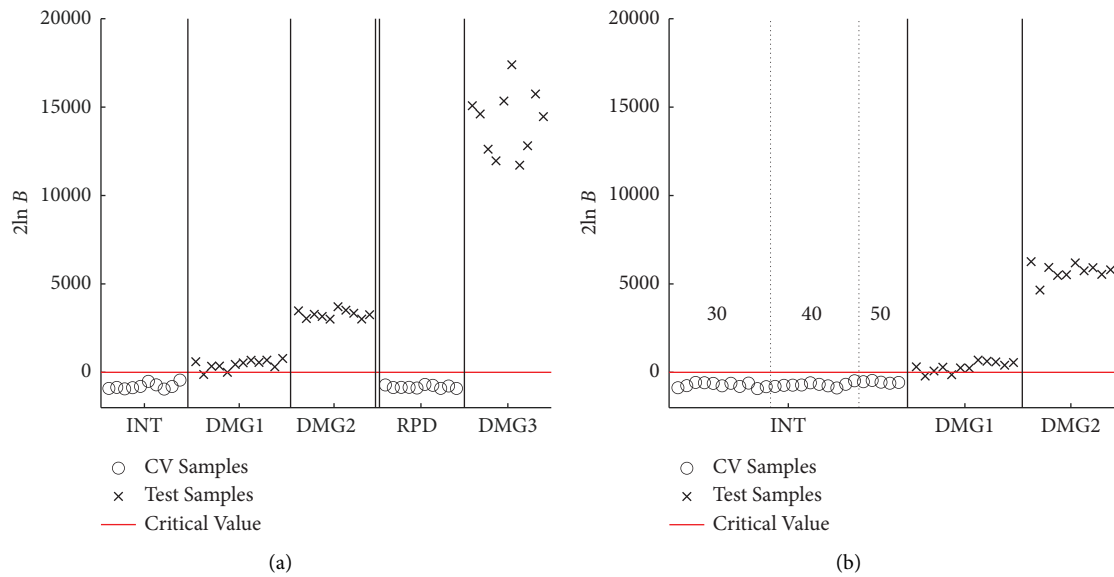
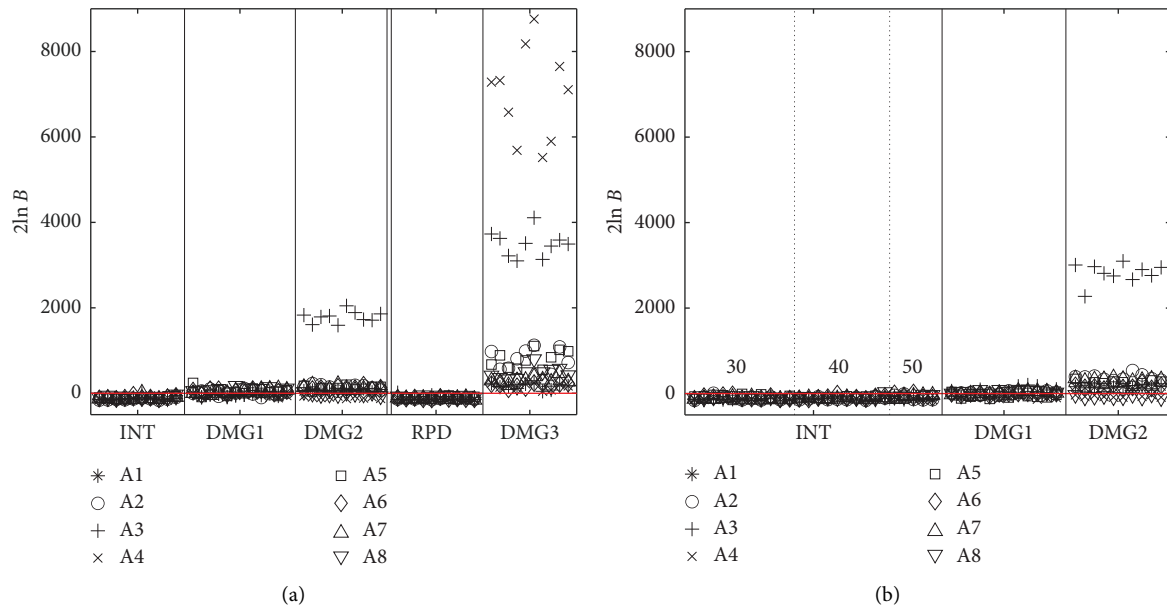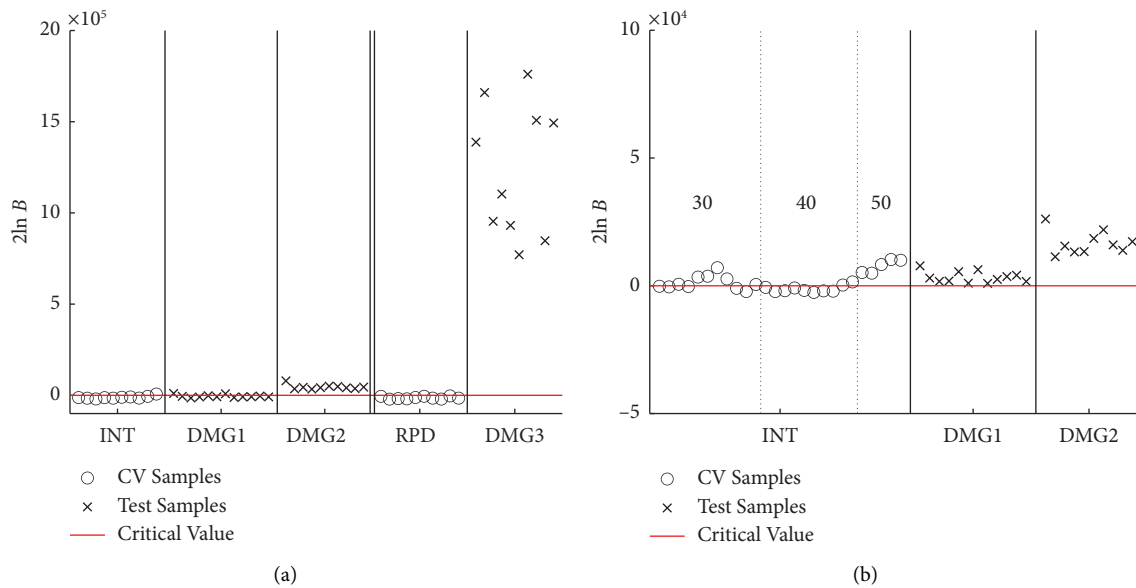FIGURE 10: Global Bayes factors: (a) for Case 1 and (b) for Case 2 (30, 40, and 50 denote vehicle speed in km/h).

and the critical value are provided similarly to those in Figure 10. In those figures, some local Bayes factors are much higher than others for DMG2 and DMG3. For DMG2, the higher values appear at measurement location A3. For DMG3, in contrast, the higher values are found at A4. The A3 and A4 are the closest measurement locations to the

TABLE 4: Summary of the global Bayes factor.

		Mean value	Correct answer ratio
Case 1	INT40	−777	10/10
	DMG1	432	10/12
	DMG2	3280	10/10
	RPD	−818	10/10
	DMG3	14175	10/10
Case 2	INT30	−721	11/11
	INT40	−630	10/10
	INT50	−696	5/5
	DMG1	307	10/12
	DMG2	5704	10/10

FIGURE 11: Local Bayes factors: (a) for Case 1 and (b) for Case 2 (30, 40, and 50 denote vehicle speed in km/h).

FIGURE 12: Bayes factors without PCA: (a) for Case 1 and (b) for Case 2 (30, 40, and 50 denote vehicle speed in km/h).

damaged member, respectively, for DMG2 and DMG3. For DMG1, the local Bayes factor is not as significant as DMG2 and DMG3. Those results demonstrate that the local Bayes factors indicate the closest measurement point to damage locations if the damage is severe enough that the member nearby the sensor thoroughly ruptures.

5. Concluding Remarks

This study proposes damage detection methods for bridges using ambient loads to cope with difficulties in decision-making for bridge maintenance. The damage detection aims to develop a screening method for numerous bridges without traffic interruption. Load-induced noise often hinders subtle changes. So, this study automates and generalizes the change detection in modal properties and proposes a simplified anomaly indicator robust against load-induced noise.

A time series of bridge accelerations provides a likelihood function of a vector autoregressive (VAR) model. The likelihood function and a noninformative prior produce the posterior distribution of the model parameters that constitute the VAR model. The posterior distribution provides a reference model representing healthy bridge vibrations using acceleration measured under healthy conditions. The orthogonal bases of the posterior distribution obtained from the principal component analysis extract damage-sensitive parameters comparable to modal properties. We formulated Bayesian hypothesis testing comparing two evidences representing the healthy and damaged state of the bridge, using the damage-sensitive parameters.

This study examined experimental data on an actual simply supported steel truss bridge with severed tension members to investigate the feasibility of the proposed approach for damage detection. The AR order is determined with the Bayesian information criterion. The contribution ratios of the principal components indicate an appropriate number of damage-sensitive parameters. The damage-sensitive parameters are converted into five bending modal properties, identical to the results of an earlier study [11].

The proposed Bayes factors result in much higher mean values than "very strong" evidence in the conventional scale for all damage considered in the case study, including the subtle change caused by the half-cut of the member. Change in the vehicle speed does not lead to a false positive result in this case study. This result suggests that the proposed methodology is robust against changes in vehicle speed compared to the existing Bayesian hypothesis testing, as discussed in Appendix B. Localized Bayes factors have significant values at the measurement locations closest to the damaged members for severe damage scenarios where the truss members were ruptured thoroughly.

We prospect the following discussions and investigations in future studies:

(i) This study validated the robustness of the proposed method against load-induced noise. However, because of the limitations of field experiments, we have not discussed the other source of noise. Especially, temperature fluctuation is one of the crucial concerns for long-term health monitoring. Future studies should follow to validate or improve the proposed method for long-term environmental change.

(ii) The proposed method evaluates the ratio of the evidence functions for damaged bridge and healthy bridge. However, we have yet to quantify the damage severity. The statistic scale proposed in a previous study, cited as Table 1, appears unavailable for damage quantification because the calculated results are much higher than it. Model-based sensitivity analysis to quantify various damages is required because the test case in the field experiment is quite limited. Also, sensitivity analysis needs to be undertaken for the local Bayes factors to confirm their sensitivity to the damages.

(iii) The damping ratios were underestimated from the damage-sensitive parameters. The possible reason is that the adopted estimation technique assumes impulse response, whereas actual loads produce continuous excitation. Modifications in models or feature extraction methods are required to detect changes in damping ratios.

(iv) Although the proposed method almost automates the procedure for damage detection, the choice of the dimension of the damage-sensitive parameters has yet to automate. The principal components' contribution ratios help engineers find how much the parameters contribute to the modal response. However, they still need to determine the dimension by themselves. Further automation is desired to avoid overlooking damage-sensitive parameters.

(v) The proposed method enables rapid screening for damage detection without any structural models. After the screening, engineers will require damage identification in the next phase. Structural-model-based techniques are likely suitable for further detailed damage localization and identification.

Appendix

A. Relationship with Classical Modal Estimation

This appendix shows that the modal properties estimated in the proposed method are consistent with the eigensystem realization algorithm (ERA) [40]. In ERA, the modal properties of the system are estimated with singular value decomposition (SVD) to a Hankel matrix, which is defined as

$$\mathbf{H}(k) = \begin{bmatrix} \mathbf{y}_{k+1} & ,\dots, & \mathbf{y}_{k+n-p} \\ \vdots & \ddots & \vdots \\ \mathbf{y}_{k+p} & ,\dots, & \mathbf{y}_{k+n-1} \end{bmatrix} = \begin{bmatrix} \boldsymbol{\phi}_{k+p+1} \cdots \boldsymbol{\phi}_{k+n} \end{bmatrix}.$$

$$(A.1)$$

As well as equation (26), with the sufficiently large n, the Hankel matrix relates to the PCA proposed in this study as follows:

$$\mathbf{H}(0)\,\mathbf{H}^{\mathrm{T}}(0) = \sum_{k=p+1}^{n} \boldsymbol{\phi}_k \boldsymbol{\phi}_k^{\mathrm{T}} \propto \mathbf{U}\boldsymbol{\Lambda}\mathbf{U}^{\mathrm{T}}. \qquad (A.2)$$

Accordingly, the left singular vector of the Hankel matrix $\mathbf{H}(0)$ is consistent with the vector composing $\mathbf{U}$ in equation (24). The singular value decomposition (SVD) is applied to $H(0)$ as

$$\mathbf{H}(0) = \mathbf{U}\boldsymbol{\Sigma}\mathbf{V}^{\mathrm{T}}. \qquad (A.3)$$

Here, $\boldsymbol{\Sigma}$ is a rectangular matrix consisting of the singular values, and $\mathbf{V}$ is an orthonormal matrix consisting of the right singular vectors. Note that $\boldsymbol{\Lambda} \propto \boldsymbol{\Sigma}\boldsymbol{\Sigma}^{\mathrm{T}}$ is satisfied because of equation (A.2). Therefore, using the first q singular values and corresponding singular vectors, $H(0)$ is approximated as

$$\mathbf{H}(0) \approx \mathbf{U}_q \boldsymbol{\Sigma}_q \mathbf{V}_q^{\mathrm{T}}, \qquad (A.4)$$

where $\boldsymbol{\Sigma}_q$, $\mathbf{U}_q$, and $\mathbf{V}_q$ are submatrices consisting of the first q singular values and singular vector.

Using the Hankel matrix, the VAR model in equation (1) is transformed as

$$\mathbf{H}(1) = \begin{bmatrix} \begin{array}{c|c} \mathbf{O}_m & \\ \vdots & \mathbf{I}_{m(p-1)} \\ \mathbf{O}_m & \\ \hline & \mathbf{W} \end{array} \end{bmatrix} \mathbf{H}(0) + \begin{bmatrix} \mathbf{O}_{m(p-1)} \\ \hline \mathbf{e}_{p+1} \quad \cdots \quad \mathbf{e}_n \end{bmatrix},$$

$$(A.5)$$

where $\mathbf{I}_i$ and $\mathbf{O}_i$ stand, respectively, for the $i \times i$ identity and zero matrices. Assuming sufficiently large n, the pseudoinverse matrix of $H(0)$ is given as

$$\mathbf{H}^{\dagger}(0) = \mathbf{H}^{\mathrm{T}}(0)\left(\mathbf{H}(0)\,\mathbf{H}^{\mathrm{T}}(0)\right)^{-1}. \qquad (A.6)$$

Since the VAR model assumes white noise, $\mathbf{e}_k$ is independent of $\boldsymbol{\phi}_k$. Therefore, using the pseudoinverse matrix, the following approximation is given:

$$\begin{bmatrix} \mathbf{e}_{p+1} & \cdots & \mathbf{e}_n \end{bmatrix} \mathbf{H}^{\dagger}(0) = \sum_{k=p+1}^{n} \mathbf{e}_k \boldsymbol{\phi}_k^{\mathrm{T}}\left(\mathbf{H}(0)\,\mathbf{H}^{\mathrm{T}}(0)\right)^{-1} \approx \mathbf{O}.$$

$$(A.7)$$

Equation (A.5) is transformed as

$$\mathbf{H}(1)\mathbf{H}^{\dagger}(0) = \begin{bmatrix} \begin{array}{c|c} \mathbf{O}_m & \\ \vdots & \mathbf{I}_{m(p-1)} \\ \mathbf{O}_m & \\ \hline & \mathbf{W} \end{array} \end{bmatrix} \qquad (A.8)$$

In ERA, the pulse response is assumed instead of white-noise excitation, i.e., $\mathbf{x}_0 = \mathbf{0}$, $\mathbf{e}_0 = [1, \ldots, 1]^{\mathrm{T}}$, and $\mathbf{e}_k = \mathbf{0}$ (for $k \geq 1$). Note that equation (A.8) is consistent both for the white noise and pulse-response assumptions.

Following the pulse-response assumption, the Hankel matrix $\mathbf{H}(1)$ is given as

$$\mathbf{H}(1) \approx \mathbf{U}_q \boldsymbol{\Sigma}_q^{1/2} \mathbf{A} \boldsymbol{\Sigma}_q^{1/2} \mathbf{V}_q^{\mathrm{T}}, \qquad (A.9)$$

where $\mathbf{A}$ is the constant matrix in equation (28). Equations (A.4), (A.8), and (A.9) produce the following $\mathbf{A}$:

$$\mathbf{A} = \boldsymbol{\Sigma}_q^{-1/2}\mathbf{U}_q^{\mathrm{T}} \begin{bmatrix} \begin{array}{c|c} \mathbf{O}_m & \\ \vdots & \mathbf{I}_{m(p-1)} \\ \mathbf{O}_m & \\ \hline & \mathbf{W} \end{array} \end{bmatrix} \mathbf{U}_q \boldsymbol{\Sigma}_q^{1/2} = \boldsymbol{\Sigma}_q^{-1/2}\mathbf{U}_q^{\mathrm{T}} \begin{bmatrix} \mathbf{U}_{q[m+1:mp]} \\ \widetilde{\mathbf{W}}_1 \end{bmatrix} \boldsymbol{\Sigma}_q^{1/2} \qquad (A.10)$$

where $\mathbf{U}_{q[a:b]}$ represents a submatrix that consists of a to b rows of matrix $\mathbf{U}_q$. The constant matrix $\mathbf{C}$ in equation (29) is estimated as

$$\mathbf{C} = \mathbf{U}_{q[1:m]} \boldsymbol{\Sigma}_q^{1/2}. \qquad (A.11)$$

For simplicity, this study adopts $\mathbf{A}$ and $\mathbf{C}$ as shown in equations (30) and (31) instead of equations (A.10) and (A.11) because the modal estimation results are not altered by omitting $\boldsymbol{\Sigma}_q$ from those equations.

B. Comparison with Existing Bayesian Hypothesis Testing

Here, Bayesian hypothesis testing without PCA is discussed for comparison. Classically, the evidence functions to calculate Bayes factors are approximated by BIC [22, 38]. The authors previously assessed the validity of this approach for SHM [47]. This appendix provides the equivalent hypothesis testing using the notation presented in Section 2 for comparison. The hypothesis testing is formulated as follows:

(i) The null hypothesis $\mathscr{H}_0$ presumes that the parameters $\mathbf{W}$ are fixed to the MLEs obtained from the reference dataset, i.e., $\mathbf{W} = \widehat{\mathbf{W}}_{\mathrm{r}}$

(ii) The alternative hypothesis $\mathscr{H}_1$ presumes $\mathbf{W} \neq \widehat{\mathbf{W}}_{\mathrm{r}}$

(iii) Parameters $\boldsymbol{\Sigma}$ are fixed to the MLEs obtained from the reference dataset $\boldsymbol{\Sigma} = \widehat{\boldsymbol{\Sigma}}_{\mathrm{r}}$

Here, likelihood functions for parameters $\mathbf{W}$ satisfy the following:

$$p\left(\mathbf{Y}_t \mid \mathbf{W}, \widehat{\mathbf{\Sigma}}_r\right) \propto \prod_{k=p+1}^{n} \mathcal{N}\left(\mathbf{y}_k^t \mid \mathbf{W}\boldsymbol{\phi}_k^t, \widehat{\mathbf{\Sigma}}_r\right) \propto \exp\left\{-\frac{1}{2}\mathrm{tr}\left[\sum_{k=p+1}^{n_t}\left(\mathbf{y}_k^t - \widehat{\mathbf{W}}_r\boldsymbol{\phi}_k^t\right)\left(\mathbf{y}_k^t - \widehat{\mathbf{W}}_r\boldsymbol{\phi}_k^t\right)^{\mathrm{T}}\widehat{\mathbf{\Sigma}}_r^{-1}\right]\right\}. \tag{B.1}$$

Therefore, the log-scaled evidence function for the null hypothesis is given as

$$2\ln p\left(\mathbf{Y}_t \mid \mathcal{H}_0\right) = -\mathrm{tr}\left[\sum_{k=p+1}^{n_t}\left(\mathbf{y}_k^t - \widehat{\mathbf{W}}_r\boldsymbol{\phi}_k^t\right)\left(\mathbf{y}_k^t - \widehat{\mathbf{W}}_r\boldsymbol{\phi}_k^t\right)^{\mathrm{T}}\widehat{\mathbf{\Sigma}}_r^{-1}\right] + \mathrm{Const.} \tag{B.2}$$

According to [48], the log-scaled evidence function for the alternative hypothesis is approximated as

$$2\ln p\left(\mathbf{Y}_t \mid \mathcal{H}_1\right) \approx -\mathrm{tr}\left[\sum_{k=p+1}^{n_t}\left(\mathbf{y}_k^t - \widehat{\mathbf{W}}_t\boldsymbol{\phi}_k^t\right)\left(\mathbf{y}_k^t - \widehat{\mathbf{W}}_t\boldsymbol{\phi}_k^t\right)^{\mathrm{T}}\widehat{\mathbf{\Sigma}}_r^{-1}\right] - m^2 p\ln\left(n_t - p\right) + \mathrm{Const}, \tag{B.3}$$

where $\widehat{\mathbf{W}}_t$ represents the following MLE obtained from the test dataset.

$$\widehat{\mathbf{W}}_t = \left(\sum_{k=p+1}^{n_t}\mathbf{y}_k^t{\boldsymbol{\phi}_k^t}^{\mathrm{T}}\right)\left(\sum_{k=p+1}^{n_t}\boldsymbol{\phi}_k^t{\boldsymbol{\phi}_k^t}^{\mathrm{T}}\right)^{-1}. \tag{B.4}$$

Equations (B.2)–(B.4) produce the following log-scaled Bayes factor:

$$2\ln B = 2\ln p\left(\mathbf{Y}_t \mid \mathcal{H}_0\right) - 2\ln p\left(\mathbf{Y}_t \mid \mathcal{H}_1\right) \approx \mathrm{tr}\left[\left(\widehat{\mathbf{W}}_r - \widehat{\mathbf{W}}_t\right)\left(\sum_{k=p+1}^{n_t}\boldsymbol{\phi}_k^t{\boldsymbol{\phi}_k^t}^{\mathrm{T}}\right)\left(\widehat{\mathbf{W}}_r - \widehat{\mathbf{W}}_t\right)^{\mathrm{T}}\widehat{\mathbf{\Sigma}}_r^{-1}\right] - m^2 p\ln\left(n_t - p\right). \tag{B.5}$$

Figures 12(a) and 12(b) show the global Bayes factors calculated with equation (B.5), respectively, for Cases 1 and 2. The results demonstrate that test datasets of DMG1 engender false negatives. That is probably because the anomaly caused by DMG1 is inconspicuous among the other model parameters. This observation indicates that the proposed method has advantages for detecting subtle changes in modal properties.

In Figure 12(b), false-positive CV samples are observed, especially in INT50. One possible reason is that the difference in the waveform shown in Figure 5(c) affects the model parameters, which are irrelevant to modal properties. Another possible explanation is the limited number of samples for INT50. Namely, nonuniformity in testing cases may produce biased results in anomaly detection. Note that the proposed method reduces the false positives. This observation indicates that the proposed method is more robust against unsteady ambient loads than the existing Bayesian hypothesis testing is.

Data Availability

The field measurement data used to support the findings of this study have been deposited in the Mendeley Data repository (https://doi.org/10.17632/sc8whx4pvm.2).

Disclosure

A part of this study has been published in the author's Ph.D. thesis [46].

Conflicts of Interest

The authors declare that there are no conflicts of interest regarding the publication of this paper.

Acknowledgments

References

[1] S. W. S. Doebling, C. R. C. Farrar, M. B. M. Prime, and D. W. D. Shevitz, *Damage Identification and Health Monitoring of Structural and Mechanical Systems from Changes in Their Vibration Characteristics: A Literature Review*, Los Alamos National Laboratory Report LA-13070-MS, Los Alamos, NM, USA, 1996.

[2] O. S. Salawu, "Detection of structural damage through changes in frequency: a review," *Engineering Structures*, vol. 19, no. 9, pp. 718–723, 1997.

[3] W. Heylen, S. Lammens, and P. Sas, *Modal Analysis Theory and Testing*, KU Leuven, Leuven, Belgium, 1997.

[4] S. D. Fassois and J. S. Sakellariou, "Time-series methods for fault detection and identification in vibrating structures," *Phil. Trans. R. Soc. A.* vol. 365, no. 1851, pp. 411–448, 2007.

[5] R. J. Savage and P. C. Hewlett, "A new NDT method for structural integrity assessment," *NDT & E International*, vol. 11, no. 2, pp. 61–67, 1978.

[6] P. Gudmundson, "Eigenfrequency changes of structures due to cracks, notches or other geometrical changes," *Journal of the Mechanics and Physics of Solids*, vol. 30, no. 5, pp. 339–353, 1982.

[7] A. K. Pandey, M. Biswas, and M. M. Samman, "Damage detection from changes in curvature mode shapes," *Journal of Sound and Vibration*, vol. 145, no. 2, pp. 321–332, 1991.

[8] A. K. Pandey and M. Biswas, "Damage detection in structures using changes in flexibility," *Journal of Sound and Vibration*, vol. 169, no. 1, pp. 3–17, 1994.

[9] A. Deraemaeker, E. Reynders, G. De Roeck, and J. Kullaa, "Vibration-based structural health monitoring using output-only measurements under changing environment," *Mechanical Systems and Signal Processing*, vol. 22, no. 1, pp. 34–56, 2008.

[10] C. W. Kim, M. Kawatani, and J. Hao, "Modal parameter identification of short span bridges under a moving vehicle by means of multivariate AR model," *Structure and Infrastructure Engineering*, vol. 8, no. 5, pp. 459–472, 2012.

[11] K. C. Chang and C. W. Kim, "Modal-parameter identification and vibration-based damage detection of a damaged steel truss bridge," *Engineering Structures*, vol. 122, pp. 156–173, 2016.

[12] B. Peeters and G. De Roeck, "One-year monitoring of the Z 24-Bridge: environmental effects versus damage events," *Earthquake Engineering & Structural Dynamics*, vol. 30, no. 2, pp. 149–171, 2001.

[13] Y. Q. Ni, Y. W. Wang, and Y. X. Xia, "Investigation of mode identifiability of a cable-stayed bridge: comparison from ambient vibration responses and from typhoon-induced dynamic responses," *Smart Structures and Systems*, vol. 15, no. 2, pp. 447–468, 2015.

[14] Y. Goi and C. W. Kim, "Mode identifiability of a multi-span cable-stayed bridge utilizing stabilization diagram and singular values," *Smart Structures and Systems*, vol. 17, no. 3, pp. 391–411, 2016.

[15] R. Brincker, L. Zhang, and P. Andersen, "Modal identification of output-only systems using frequency domain decomposition," *Smart Materials and Structures*, vol. 10, no. 3, pp. 441–445, 2001.

[16] J. X. Mao, H. Wang, Y. G. Fu, and B. F. Spencer, "Automated modal identification using principal component and cluster analysis: application to a long-span cable-stayed bridge," *Structural Control and Health Monitoring*, vol. 26, no. 10, Article ID e2430, 2019.

[17] K. K. Nair, A. S. Kiremidjian, and K. H. Law, "Time series-based damage detection and localization algorithm with application to the ASCE benchmark structure," *Journal of Sound and Vibration*, vol. 291, no. 1–2, pp. 349–368, 2006.

[18] C. W. Kim, R. Isemoto, K. Sugiura, and M. Kawatani, "Structural fault detection of bridges based on linear system parameter and MTS method," *Journal of JSCE*, vol. 1, no. 1, pp. 32–43, 2013.

[19] C. W. Kim, K. C. Chang, S. Kitauchi, and P. J. McGetrick, "A field experiment on a steel Gerber-truss bridge for damage detection utilizing vehicle-induced vibrations," *Structural Health Monitoring*, vol. 15, no. 2, pp. 174–192, 2016.

[20] Q. W. Zhang, "Statistical damage identification for bridges using ambient vibration data," *Computers & Structures*, vol. 85, no. 7–8, pp. 476–485, 2007.

[21] Y. Goi and C. W. Kim, "Damage detection of a truss bridge utilizing a damage indicator from multivariate autoregressive model," *Journal of Civil Structural Health Monitoring*, vol. 7, no. 2, pp. 153–162, 2017.

[22] C. M. Bishop, *Pattern Recognition and Machine Learning*, Springer, Berlin, Germany, 2006.

[23] K. V. Yuen and L. S. Katafygiotis, "Bayesian fast Fourier transform approach for modal updating using ambient data," *Advances in Structural Engineering*, vol. 6, no. 2, pp. 81–95, 2003.

[24] S. K. Au, F. L. Zhang, and Y. C. Ni, "Bayesian operational modal analysis: theory, computation, practice," *Computers & Structures*, vol. 126, pp. 3–14, 2013.

[25] H. F. Lam, J. H. Yang, and S. K. Au, "Markov chain Monte Carlo-based Bayesian method for structural model updating and damage detection," *Structural Control and Health Monitoring*, vol. 25, no. 4, Article ID e2140, 2018.

[26] X. Jiang and S. Mahadevan, "Bayesian wavelet methodology for structural damage detection," *Structural Control and Health Monitoring*, vol. 15, no. 7, pp. 974–991, 2008.

[27] R. Kass and A. Raftery, "Bayes factors," *Journal of the American Statistical Association*, vol. 90, no. 430, pp. 773–795, 1995.

[28] X. D. Sun, X. Y. Sun, J. He, and G. L. Hou, "Bayesian-based structural damage detection on the integration of global and local information," *Advances in Structural Engineering*, vol. 18, no. 4, pp. 543–553, 2015.

[29] E. Figueiredo, L. Radu, K. Worden, and C. R. Farrar, "A Bayesian approach based on a Markov-chain Monte Carlo method for damage detection under unknown sources of variability," *Engineering Structures*, vol. 80, pp. 1–10, 2014.

[30] Z. Dzunic, J. G. Chen, H. Mobahi, O. Büyüköztürk, and J. W. Fisher, "A Bayesian state-space approach for damage detection and classification," *Mechanical Systems and Signal Processing*, vol. 96, pp. 239–259, 2017.

[31] M. F. Silva, A. Santos, R. Santos, E. Figueiredo, and J. C. W. A. Costa, "Damage-sensitive feature extraction with stacked autoencoders for unsupervised damage detection," *Structural Control and Health Monitoring*, vol. 28, no. 5, Article ID e2714, 2021.

[32] S. Arangio and J. L. Beck, "Bayesian neural networks for bridge integrity assessment," *Structural Control and Health Monitoring*, vol. 19, no. 1, pp. 3–21, 2012.

[33] M. Markou and S. Singh, "Novelty detection: a review – part 1: statistical approaches," *Signal Processing*, vol. 83, no. 12, pp. 2481–2497, 2003.

[34] M. A. F. Pimentel, D. A. Clifton, L. Clifton, and L. Tarassenko, "A review of novelty detection," *Signal Processing*, vol. 99, pp. 215–249, 2014.

[35] E. Akintunde, S. Eftekhar Azam, A. Rageh, and D. G. Linzell, "Unsupervised machine learning for robust bridge damage detection: full-scale experimental validation," *Engineering Structures*, vol. 249, Article ID 113250, 2021.

[36] A. I. Ozdagli and X. Koutsoukos, "Machine learning based novelty detection using modal analysis," *Computer-Aided Civil and Infrastructure Engineering*, vol. 34, no. 12, pp. 1119–1140, 2019.

[37] D. Sen, K. Erazo, W. Zhang, S. Nagarajaiah, and L. Sun, "On the effectiveness of principal component analysis for decoupling structural damage and environmental effects in bridge structures," *Journal of Sound and Vibration*, vol. 457, pp. 280–298, 2019.

[38] G. Schwarz, "Estimating the dimension of a model," *Annals of Statistics*, vol. 6, no. 2, pp. 461–464, 1978.

[39] P. van Overschee and B. De Moor, *Subspace Identification for Linear Systems*, Kluwer Academic Publishers, Norwell, Massachusetts, United States, 1996.

[40] J. N. Juang and R. S. Pappa, "An eigensystem realization algorithm for modal parameter identification and model reduction," *Journal of Guidance, Control, and Dynamics*, vol. 8, no. 5, pp. 620–627, 1985.

[41] C. W. Kim, F. L. Zhang, K. C. Chang, P. J. McGetrick, and Y. Goi, "Ambient and vehicle-induced vibration data of a steel truss bridge subject to artificial damage," *Journal of Bridge Engineering*, vol. 26, no. 7, Article ID 04721002, 2021.

[42] X. He and G. De Roeck, "System identification of mechanical structures by a high-order multivariate autoregressive model," *Computers & Structures*, vol. 64, no. 1-4, pp. 341–351, 1997.

[43] H. Jeffreys, "An invariant form for the prior probability in estimation problems," *Proceedings of the Royal Society of London, Series A: Mathematical and Physical Sciences*, vol. 186, no. 1007, pp. 453–461, 1946.

[44] K. Yamada, "An advice from rupture into a diagonal member of Kisogawa bridge," *JSCE Mag Civil Eng.,* vol. 93, no. 1, pp. 29-30, 2008.

[45] C. W. Kim, F. L. Zhang, K. C. Chang, P. McGetrick, and Y. Goi, "Old ADA Bridge-damage vibration data," *Mendeley Data*, vol. 2, 2021.

[46] Y. Goi, *Bayesian damage detection for vibration based bridge health monitoring*, Ph.D. thesis, Kyoto University, Kyoto, Japan, 2018.

[47] Y. Goi and C. W. Kim, "Bayesian outlier detection for health monitoring of bridges," *Procedia Engineering*, vol. 199, pp. 2120–2125, 2017.

[48] R. E. Kass and L. Wasserman, "A reference Bayesian test for nested hypotheses and its relationship to the Schwarz criterion," *Journal of the American Statistical Association*, vol. 90, no. 431, pp. 928–934, 1995.